mTOR-regulated Mitochondrial Metabolism Limits Mycobacterium-induced Cytotoxicity

Antonio J. Pagán[1,2,3], Lauren J. Lee[1,2], Joy Edwards-Hicks[4,6], Cecilia B. Moens[5], David M. Tobin[3,7], Elisabeth M. Busch-Nentwich[1,8], Erika L. Pearce[4,9], Lalita Ramakrishnan[1,2,3,10]

[1]Molecular Immunity Unit, Cambridge Institute of Therapeutic Immunology and Infectious Diseases, Department of Medicine, University of Cambridge, Cambridge CB2 0AW, UK.

[2]MRC Laboratory of Molecular Biology, Cambridge CB2 0QH, UK

[3]Department of Microbiology, University of Washington, Seattle, WA 98195, USA

[4]Max Planck Institute of Immunobiology and Epigenetics, Freiburg im Breisgau, Germany.

[5]Division of Basic Sciences, Fred Hutchinson Cancer Center, Seattle, WA 98109, USA

[6]Present address: Cambridge Institute of Therapeutic Immunology and Infectious Diseases, Department of Medicine, University of Cambridge, Cambridge CB2 0AW, UK

[7]Present address: Department of Molecular Genetics and Microbiology, Duke University, Durham, NC 27710, USA

[8]Present address: School of Biological and Behavioural Sciences, Faculty of Science and Engineering, Queen Mary University of London, London E1 4NS, UK.

[9]Present address: The Bloomberg-Kimmel Institute for Cancer Immunotherapy, Johns Hopkins University School of Medicine, Baltimore, Maryland, USA; Department of Oncology, Johns Hopkins University School of Medicine, Baltimore, MD 21287, USA.

[10]Lead contact

Correspondence: apagan@mrc-lmb.cam.ac.uk; lalitar@mrc-lmb.cam.ac.uk

ABSTRACT

Necrosis of macrophages in the tuberculous granuloma represents a major pathogenic event in tuberculosis. Through a zebrafish forward genetic screen, we identified the mTOR kinase, a master regulator of metabolism, as an early host resistance factor in tuberculosis. We found that mTOR complex 1 protects macrophages from mycobacterium-induced death by enabling infection-induced increases in mitochondrial energy metabolism fueled by glycolysis. These metabolic adaptations are required to prevent mitochondrial damage and death caused specifically by ESAT-6, the principal secreted substrate of the specialized mycobacterial secretion system ESX-1, a key virulence mediator. Thus, the host can effectively counter this early critical mycobacterial virulence mechanism simply by regulating energy metabolism, allowing pathogen-specific immune mechanisms time to develop. Our findings may explain why *Mycobacterium tuberculosis*, albeit humanity's most lethal pathogen, is successful in only a minority of infected individuals.

INTRODUCTION

Mycobacterium tuberculosis (Mtb) induces the formation of granulomas, organized structures comprised of macrophages, within which mycobacteria reside, and accessory cells (Pagan and Ramakrishnan, 2014; 2018; Ramakrishnan, 2012). This hallmark immunological structure of tuberculosis (TB) represents a key host-pathogen battleground that determines the outcome of infection (Pagan and Ramakrishnan, 2014; Ramakrishnan, 2012). In the majority of individuals, the granuloma is successful in clearing Mtb infection, often leaving a residual, sterile, fibrotic structure as a stamp of past infection (Behr et al., 2018; 2019; Behr et al., 2021; Canetti et al., 1972; Feldman and Baggenstoss, 1938; Opie and Aronson, 1927; Terplan, 1951). In contrast, in the minority of individuals who go on to develop TB, the granuloma is often rendered a mycobacterium-beneficial structure that promotes bacterial expansion and dissemination (Pagan and Ramakrishnan, 2014; Ramakrishnan, 2012). Granuloma necrosis constitutes a pivotal pathogenic event because it delivers macrophage-resident mycobacteria into the extracellular milieu, which increases their replication by overcoming the growth restriction imposed by macrophage immune defenses (Pagan and Ramakrishnan, 2014; Ramakrishnan, 2012; Russell, 2007). Necrosis of lung granulomas with their attendant rupture into the airways also facilitates transmission, sustaining the global TB burden and promoting Mtb's evolutionary survival (Ong et al., 2014; Ramakrishnan, 2012). Exploitation of the granuloma begins in the innate stage of the response, enabling Mtb to gain a foothold in the host (Cambier et al., 2014a; Pagan and Ramakrishnan, 2014; Ramakrishnan, 2012). Innate immune defects that facilitate mycobacterial exploitation of the granuloma, including accelerated granuloma necrosis,

may hinder the development of host-protective adaptive immune responses. Conversely, as adaptive immunity elaborates inflammatory programs set in motion by innate immunity, it likely contributes to TB progression through the amplification of pathogenic innate inflammatory responses (Pagan and Ramakrishnan, 2014; 2018). Thus, the extent of mycobacterial exploitation of the granuloma — from its inception and throughout the infection — may influence TB disease course.

Zebrafish infected with *Mycobacterium marinum* (Mm), a close relative of Mtb develop a TB-like disease featuring the necrotic granulomas of human TB (Cosma et al., 2003; Swaim et al., 2006). Mm-infected zebrafish larvae, in which adaptive immunity has not yet developed, also develop disease with organized granulomas that undergo necrosis (Davis et al., 2002). Thus, the zebrafish larva offers the opportunity to dissect the sole contribution of innate immunity in tuberculous granuloma formation and necrosis (Davis *et al.*, 2002; Davis and Ramakrishnan, 2009; Ramakrishnan, 2013; 2020). The larva's optical transparency and genetic tractability enables the detailed, sequential monitoring by intravital microscopy of the steps of infection, the contribution of host and pathogen determinants to them, and the consequences to outcome (Ramakrishnan, 2013). The use of unbiased genetic screens and candidate gene approaches in zebrafish larvae has shed light on granuloma biology (Ramakrishnan, 2013; 2020). In particular, hypersusceptible zebrafish mutants displaying accelerated granuloma necrosis have identified innate immune host determinants that protect against necrosis and that are relevant in the context of human TB (Berg et al., 2016; Clay et al., 2008; Pagan et al., 2015; Roca and Ramakrishnan, 2013; Roca et al., 2019; Tobin et al., 2012; Tobin et al., 2010; Whitworth et al., 2021a; Whitworth et al., 2021b).

Here, we report on insights into TB pathogenesis and resistance gained from studies on a loss-of-function mutant in mTOR kinase that exhibits rapid granuloma necrosis. The mTOR pathway integrates environmental signals emanating from diverse nutrient-sensing and growth factor receptor pathways to regulate biosynthetic and metabolic processes vital for cellular development, growth, survival, and function (Liu and Sabatini, 2020). Iterative experimental approaches in the zebrafish and in human macrophages uncover the mitotoxic function of mycobacterial ESAT-6 and show that mTOR-facilitated mitochondrial metabolism serves as a highly effective innate 'counter virulence' factor in TB by exerting a mitoprotective effect against this critical mycobacterial virulence factor.

RESULTS

mTORC1 Deficiency Confers Susceptibility to Mm Infection in Zebrafish

The zebrafish mutant *fh178*, identified in a forward genetic screen (Tobin *et al.*, 2010), was hypersusceptible to Mm, with larvae exhibiting increased bacterial burdens relative to wild-type and heterozygote siblings following intravenous infection into the caudal vein (CV) (Figures 1A-1C). By four days post infection (dpi), *fh178* mutant granulomas had depleted their macrophages, with the released bacteria growing exuberantly, forming the rope-like cords that are characteristic of extracellular growth (Pagan *et al.*, 2015; Tobin *et al.*, 2010) (Figure 1D and 1E). Mycobacterial cording, a sensitive and specific surrogate for macrophage depletion, is a readily quantifiable, binary phenotype for mapping mutants rendered hypersusceptible by granuloma necrosis (Berg *et al.*, 2016; Tobin *et al.*, 2010). Using simple sequence length polymorphism markers, we

thus mapped the *fh178* mutation to a nonsense mutation in exon 24 of the *mtor* gene. We confirmed that genetic disruption of *mtor* was the cause of *fh178* hypersusceptibility by showing that animals with a nonsense mutation in exon 19 (*mtor*^{sa16755} identified in the Zebrafish Mutation Project (Kettleborough et al., 2013)) also exhibited hypersusceptibility with cording as did compound *fh178/sa16755* heterozygotes (Figure 1F and 1G).

The mTOR kinase functions in two distinct molecular complexes, mTORC1 and mTORC2, that require the adaptors Raptor and Rictor for their assembly, respectively (Liu and Sabatini, 2020). Animals with nonsense alleles of *rptor*, the gene encoding Raptor, showed similar cording as the *mtor* mutants, whereas those with nonsense alleles of the zebrafish orthologs of mammalian *Rictor*, *rictora* and *rictorb*, did not (Figure 1H and 1I). Pharmacological inhibition of mTOR or mTORC1 with torin1 or rapamycin, respectively (Benjamin et al., 2011), recapitulated genetic mTOR/mTORC1 deficiency with increased cording (Figure 1J). Thus, mTORC1 deficiency confers susceptibility to mycobacterial infection, linked to early granuloma breakdown. Because zebrafish larvae have not yet developed adaptive immunity, this reflects resistance conferred by mTOR in the sole context of innate immunity.

mTOR Deficiency Accelerates Death of Mycobacterium-Infected Macrophages

At 4 dpi, wild-type animals had granulomas with sparse intracellular bacteria; in contrast mTOR-deficient animals had clusters of extracellular bacteria (Figure 1D). These extracellular clusters had similar shapes to wild-type granulomas (Figure 1D, compare top and bottom), suggesting that granulomas had formed initially and then broken down

due to macrophage death. To detail the kinetics of macrophage death, we infected zebrafish larvae in the hindbrain ventricle (HBV), an acellular compartment lined with a single layer of epithelium that allows detailed monitoring of macrophage recruitment and granuloma formation (Davis and Ramakrishnan, 2009) (Figure 1A). Rapamycin-treated animals formed tight aggregates of infected macrophages similar to wild-type by 2 dpi (Figure 2A). However, the next day, most macrophages in the nascent granulomas of the rapamycin-treated animals had died, leaving a clump of extracellular bacteria (Figure 2A).

A ready explanation for these findings could have been that, since mTORC1 signaling is required for myeloid cell development and maintenance, its deficiency would create a basal macrophage deficit leading to susceptibility (Deng et al., 2017; Karmaus et al., 2017; Lee et al., 2017; Mercalli et al., 2006; Sinclair et al., 2017; Weichhart et al., 2015). We had previously identified susceptibility from a basal macrophage deficit. We had found that zebrafish larvae deficient in the myeloid growth factor Colony Stimulating Factor-1 Receptor (CSF-1R) are susceptible to Mm infection because they have a reduced reservoir of uninfected macrophages available to replenish mycobacterium-overladen macrophages dying in granulomas (Pagan *et al.*, 2015). Further supporting this possibility, mTORC1 promotes myelopoiesis at least in part through CSF-1R signaling (Karmaus *et al.*, 2017), and mTORC1 (*rptor*)-deficient zebrafish did have reduced macrophage numbers in mock-infected animals (Figure 2B). However, although mTORC1-deficient animals had more macrophages at baseline than CSF-1R-deficient animals, their granulomas broke down at an earlier time-point: bacterial cording occurred between days two and four in mTORC1-deficient animals versus

between days five and seven in CSF-1R-deficient animals (Pagan *et al.*, 2015)(Figure 2C). This suggested that mTOR deficiency induces death of infected granuloma macrophages independently of reducing basal macrophage supply.

To show this definitively, we used time-lapse microscopy to capture in real-time the death of infected wildtype and mTOR-deficient macrophages. If mTOR-deficient granulomas are breaking down due to reduced macrophage replenishment, then dying mTOR mutant macrophages should have bacterial burdens similar to or greater than wild-type. This would also be the case if mTOR deficiency reduced the microbicidal capacity of macrophages, so that dying macrophages would be overladen with bacteria. To directly assess bacterial burdens in dying macrophages, we used blue fluorescent Mm to infect mTOR-deficient animals and their wild-type siblings that had red fluorescent macrophage membranes. All animals were also transgenic for a ubiquitously-expressed secreted annexin V tagged with yellow fluorescent protein (*Tg(ubb:secA5-YFP)*), which accumulates on the surface of cells undergoing apoptosis and other modes of regulated cell death (Bendall and Green, 2014). We monitored macrophage death by the appearance of annexin V-YFP labeling of the plasma membrane and membrane blebs followed by the loss of tdTomato fluorescence reflecting plasma membrane disintegration (Figure 2D and Movie S1). In 2 dpi animals, over a 4.5-hour imaging period that captured similar numbers of infected macrophages in mTOR-deficient and wildtype siblings, 6-fold more mTOR-deficient macrophages died (Figure 2E and 2F and Movie S2). Importantly, mTOR-deficient macrophages died with lower bacterial burdens than mTOR-sufficient macrophages than wild-type (Figure 2G),

suggesting that they are “intolerant” of mycobacterial infection. These findings also ruled out the possibility that mTOR deficiency causes a macrophage microbicidal defect.

Next, to determine if mTOR’s protective effect was macrophage-intrinsic, we compared mTOR mutant and wild-type macrophages in the same environment by creating wildtype – mTOR mutant parabionts with differentially labeled macrophages, red and yellow fluorescent in wild-type and mTOR mutants, respectively and infecting both caudal veins (Figure 2H). By 4 dpi, mTOR mutant macrophages had been depleted by more than 90% on both wild-type and mTOR mutant sides of the parabionts, whereas wild-type macrophages persisted equally on both sides (Figure 2I). The depletion of mTOR mutant macrophages in these animals should not lead to Mm cording because the complement of WT macrophages should be able to efferocytose the infected mTOR mutant corpses and keep Mm intracellularly. By 4 dpi, as predicted, Mm was only found inside the WT macrophages (Figure 2J). In mTOR heterozygote – wildtype parabionts, mTOR heterozygote yellow fluorescent macrophages survived as well as wild-type red fluorescent macrophages, ruling out expression of the *Tg(mpeg1:YFP)* transgene as an artifactual cause of macrophage depletion of mTOR mutant macrophages (Figure 2K - 2L).

Thus, mTOR confers cell-intrinsic protection to macrophages against mycobacterium-induced death from early on even when intracellular bacteria are sparse.

Infected macrophage death in mTOR deficiency is associated with reduced membrane potential

Impairment in nutrient sensing pathways caused by mTOR-deficiency could sensitize cells to autophagic death or to mitochondrial apoptosis (Gonzalez et al., 2020; Green and Levine, 2014; Hosoi et al., 1999; Muthukkumar et al., 1995). To assess autophagic death, we created zebrafish deficient in the essential autophagy protein ATG12 (Bento et al., 2016). Macrophages in ATG12-deficient animals had defective autophagosome formation as evidenced by reduced aggregation of the autophagy protein LC3 (Figures S1A and S1B). However, ATG12 deficiency did not prevent death of mycobacterium-infected macrophages in animals rendered mTOR-deficient by rapamycin treatment (Figure S1C). Next, to assess mitochondrial apoptosis, we used caspase-9 deficient zebrafish mutants (Galluzzi et al., 2016). Capase-9 mutants had the expected defect in developmental apoptosis as reflected by reduced dead cell debris in the brain at 3 dpf (S1D and S1E). However, rapamycin treatment still induced death of their infected macrophages (Figure S1F). Thus, mTOR deficiency kills infected macrophages independent of inducing autophagy or apoptosis.

Mycobacterium-induced macrophage death typically occurs with high intracellular bacterial burdens (Amaral et al., 2019; Beckwith et al., 2020; Clay *et al.*, 2008; Lee et al., 2011), whereas mTOR-deficient macrophages died rapidly upon infection when intracellular mycobacterial burdens were still low. In previous work, we had identified macrophage death associated with low mycobacterial burdens and found it to be mediated through a pathway activated by dysregulated Tumor Necrosis Factor (TNF) (Roca and Ramakrishnan, 2013; Roca *et al.*, 2019). We found that mTOR-deficient macrophage death did not involve this pathway; inhibition of essential components, the kinase RIPK1 and the L type calcium channels, failed to rescue death (Figure S1G -

S1I). However, interrogating this pathway gave us a clue. TNF-mediated death of mycobacterium-infected macrophages is initiated by high mitochondrial reactive oxygen species (mROS) (Roca and Ramakrishnan, 2013; Roca *et al.*, 2019), whereas in mTOR deficient animals, both uninfected and infected macrophages had *lower* baseline mROS levels than in wild-type (Figure 3A and B). Moreover, while mTOR-deficient macrophages did mount the expected infection-induced increase in mROS, it was lower than wild-type (1.6-fold versus 2.1-fold) (Figure 3B). Macrophage death associated with low mROS levels implicated impaired mitochondrial function, which would be consistent with mTOR's role in regulating mitochondrial biology (Cunningham et al., 2007; Liu and Sabatini, 2020; Morita et al., 2013; Rambold and Pearce, 2018; Schieke et al., 2006).

To further explore the link between mTOR-deficiency, impaired mitochondrial bioenergetics and death of infected macrophages, we rendered the THP-1 human macrophage cell line mTOR-deficient by overnight treatment with the mTOR inhibitor torin1 prior to infection. As with the zebrafish, there was increased death of infected mTOR-deficient macrophages one day post-infection as shown by flow cytometry after staining with the cell membrane-impermeant fixable viability dye eFluor 660 (Figure 3C and 3D). Increases in mROS are linked to increased mitochondrial membrane potential (Murphy, 2009), and accordingly, flow cytometry after tetramethylrhodamine, ethyl ester (TMRE) staining showed that the infected wild-type macrophages had increased TMRE (Figure 3E and 3F). As was the case with mROS levels, mTOR-deficient macrophages had a lower baseline TMRE, which increased with infection but not to the extent in wild-type infected cells (Figure 3E and F).

Finally, death of infected mTOR signaling-deficient macrophages was associated with mitochondrial damage — a greater proportion of the infected cells had released cytochrome c (Figure 3G and 3H). In contrast, there was hardly any cytochrome c release in the uninfected cells (Figure 3G and 3H). In sum, our findings suggest that mycobacterium infection of mTOR-deficient zebrafish and human macrophages rapidly induces a mitochondrial mode of death that is associated with reduced mitochondrial metabolic activity.

mTOR Deficiency Sensitizes Macrophages to Mycobacterium-Induced Death by Impairing Glycolysis-dependent Oxidative Phosphorylation (OXPHOS)

mTOR regulates a number of metabolic pathways that, in turn, regulate mitochondrial metabolism (Liu and Sabatini, 2020). We confirmed that mTOR inhibition of THP-1 cells caused the expected reduced activity in glucose metabolism (glycolysis and the pentose phosphate pathway) and the Krebs cycle (Duvel et al., 2010; Morita *et al.*, 2013), reflected by lower metabolite abundance for these pathways consistent with reduced glycolytic and respiratory capacity (Figure S2A - S2G). The lower basal, ATP-coupled and maximal respiration, and spare respiratory capacity reflected broadly compromised mitochondrial respiration and ATP production and reduced ability to boost mitochondrial respiration in response to increased ATP demands. Together, these findings suggested that mTOR deficiency impairs mitochondrial respiration by reducing glycolysis. Consistent with this, selective inhibition of glycolysis with the glucose analog 2-deoxy-D-glucose (2DG), which inhibits hexokinase and glucose-6-phosphate isomerase function upon intracellular conversion into 2-deoxy-D-glucose-6-phosphate (Pajak et al., 2019)

reduced Krebs cycle metabolites and mitochondrial respiration (Figure S2A, S2H, and S2I and Table S1). Moreover, glycolysis-deficient macrophages had similar reductions in ATP to mTOR-deficient ones (Figure S2J).

Our findings were consistent with a model where mTOR-facilitated glycolytic fueling of the Krebs cycle sustains mitochondrial energy production required to protect infected macrophages from dying. If so, then inhibition of glycolysis should phenocopy mTOR deficiency, causing selective death of infected macrophages with impaired infection-induced increase in mitochondrial membrane potential. 2DG treatment induced both phenotypes in THP1 cells, similar to Torin1 treatment (Figure 4A and 4B). We confirmed that mTOR and glycolysis have a cytoprotective effect in Mtb infection as well. For this, we assessed macrophage death in after infection with an isogenic leucine and pantothenate auxotrophic mutant of the virulent H37Rv Mtb strain, a biosafety 2 level pathogen that elicits similar inflammatory responses and triggers diverse cell death programs (Beckwith *et al.*, 2020; Mouton et al., 2019; Roca *et al.*, 2019; Sampson et al., 2004; Sampson et al., 2011). Mtb infection caused increased death of both mTOR-deficient and glycolysis-deficient THP-1 cells (Figure 4C). Finally, in the zebrafish we found that 2DG treatment depleted infected macrophages selectively (Figure 4D-4F and Movie S3), and that this was associated with increased bacterial cording (Figure 4G). Thus, our findings suggest that mTOR exerts its cytoprotective effect by supporting glycolysis both in Mm zebrafish infection and Mm- and Mtb-infected human macrophages.

Since glycolysis contributes to mitochondrial ATP production by supplying pyruvate to the Krebs cycle (Ryan and O'Neill, 2020), intercepting this step should also

produce bacterial cording. To test this, we treated zebrafish with the mitochondrial pyruvate carrier inhibitor UK5099 (Halestrap, 1975). UK5099 treatment increased bacterial cording (Figure 4H). Glycolysis also feeds the pentose phosphate pathway (Patra and Hay, 2014), and we had observed alterations in pentose phosphate pathway metabolites after inhibition of mTOR and glycolysis (Figure S2A). However, zebrafish mutants deficient in glucose-6-phosphate dehydrogenase (G6PD), the rate-limiting enzyme of the pentose phosphate pathway, which had 90% reduction in G6PD activity, did not have increased bacterial cording (Figure 4I and 4J). This ruled out the involvement of the pentose phosphate pathway in mTOR's protective effect. Together, these results suggest that mTOR deficiency sensitizes macrophages to Mm-induced mitochondrial damage and death by impairing glycolysis-dependent OXPHOS and thereby mitochondrial energy production. Consistent with this model, we found that infection boosted ATP production within 24 hours in control macrophages (Figure 4K). In contrast, mTOR-deficient macrophages had slightly lower baseline ATP production, with infection increasing it only up to baseline wild-type levels (Figure 4K). This finding recapitulates the findings with mROS and TMRE where mTOR-deficient macrophages are able to mount a response to infection that equals or exceed wild-type baseline levels but falls short of wild-type responses upon infection. Together, these findings suggest that the increases in mitochondrial energy production in infected macrophages are necessary to protect against mycobacterium-mediated mitochondrial damage. mTOR protects against macrophage mitochondrial damage and death by enabling these infection-induced metabolic adaptations.

mTOR-dependent Glycolysis and OXPHOS Enable Macrophages to Resist Mycobacterium ESAT-6-mediated Death

The mTOR mutant had unmasked the potential of pathogenic mycobacteria to cause lethal mitochondrial damage in infected macrophages. We hypothesized that a specific mycobacterial determinant caused this damage, and our prime candidate was the ESX-1 secretion system. ESX-1 is a major mycobacterial virulence determinant which, even in normal (mTOR-sufficient) conditions, is implicated in mycobacterium-induced macrophage death and mitochondrial damage (Conrad et al., 2017; Davis and Ramakrishnan, 2009; Groschel et al., 2016; Guinn et al., 2004; Lienard et al., 2020; Simeone et al., 2012; Simeone et al., 2021; Volkman et al., 2004; Wiens and Ernst, 2016). While ESX-1 does promote pathogenic death of mTOR-sufficient macrophages, it is much more limited and occurs only when high intramacrophage bacterial burdens are reached (Davis and Ramakrishnan, 2009; Volkman *et al.*, 2004). We hypothesized that mTOR-deficiency sensitizes macrophages to ESX-1-mediated mitochondrial damage and cell death. Consistent with our hypothesis, mTOR-deficient THP-1 macrophages infected with ESX-1-deficient Mm did not have mitochondrial damage nor increased death (Figure 5A and 5B). Furthermore, in mTOR-deficient zebrafish infected with ESX-1-deficient Mm, time-lapse microscopy showed that infected macrophages did not die (Figure 5C and Supplementary Movie 4). Accordingly, the animals did not exhibit bacterial cording (Figure 5D). Finally, ESX-1-deficient infection did not cause macrophage death in 2DG-treated and UK5099-treated animals either (Figure 5E and 5F). Thus, mTOR-dependent glycolysis and OXPHOS specifically counter ESX-1-dependent mitochondrial damage and cell death.

ESX-1-mediated damage of mycobacterium-containing phagosomes is thought to be upstream of its other virulence-related phenotypes such as macrophage death and mitochondrial damage (Lienard *et al.*, 2020; Simeone *et al.*, 2012; Simeone *et al.*, 2021). The mycobacterial cell surface lipid phthiocerol dimycocerosate (PDIM) facilitates ESX-1-mediated phagosomal damage and cytotoxicity (Augenstreich et al., 2017; Lerner et al., 2018; Osman et al., 2020; Quigley et al., 2017; Simeone *et al.*, 2021) (Figure S3). We found that mTOR-deficient macrophages were similarly resistant to mycobacteria deficient in the PDIM transporter MmpL7 (Cambier et al., 2014b) — mmpL7 mutants did not induce cording in mTOR mutants (Figure 5G). We further tested mycobacterial mutants for the virulence determinants Erp and the serine protease MarP, virulence determinants that promote intramacrophage growth through distinct mechanisms from ESX-1(Berthet et al., 1998; Cosma et al., 2006; Ehrt et al., 2015; Levitte et al., 2016; Small et al., 2013; Vandal et al., 2008). We confirmed that in wild-type animals, the Erp and MarP mutants induced significantly more phagosomal damage than ESX-1 and mmpL7 mutants, as determined by staining with an antibody to galectin-8, a cytosolic protein that binds to lumenal β-galactoside-containing glycans that become exposed on damaged vesicles (Figure S3) (Osman *et al.*, 2020; Randow and Youle, 2014). Despite their intramacrophage growth attenuation (Cosma *et al.*, 2006; Levitte *et al.*, 2016), these mutants caused accelerated macrophage death in mTOR-deficient animals (Figure 5G). These findings implicate ESX-1-dependent phagosomal permeabilization in the accelerated death of mTOR-deficient macrophages.

ESX-1's membranolytic activity had been ascribed to its major secreted substrate ESAT-6 (6 kDa early secretory antigenic target); however, pinning down its role versus

those of other ESX-1 substrates has been complicated by their co-dependency for secretion, as deletion of ESAT-6 causes loss of other ESX-1 substrates (Bao et al., 2021; Champion et al., 2014; Fortune et al., 2005). Recent work has pinpointed a specific role for ESAT-6 in phagosomal damage and virulence, by identifying point mutations in ESAT-6 that allow substantial levels of secretion of ESAT-6 and other ESX-1 substrates yet cause loss of phagosomal membrane damage and/or virulence (Brodin et al., 2005; Osman et al., 2022; Zhang et al., 2016). To test the specific role of ESAT-6-induced phagosomal damage in mediating cell death in mTOR deficiency, we used *esxA* mutant Mm expressing either of two such ESAT-6 C-terminal point mutations, M83I and M93T (Brodin *et al.*, 2005; Osman *et al.*, 2022). Mm-ESAT-6^{M83I} and Mm-ESAT-6^{M93T} infections did not kill macrophages in mTOR-deficient zebrafish (Figure 5H). These findings bolster the conclusion that mycobacterium-induced phagosomal damage is an absolute requirement for the cell death induced by mTOR deficiency and specifically implicate the ESX-1 substrate ESAT-6.

mTOR Enables Infected Macrophages to specifically resist ESX-1-mediated mitochondrial damage

We considered the possibility that mTOR-deficiency simply sensitizes macrophage phagosomes to ESX-1-mediated damage. However, mTOR-deficient and wildtype macrophages had similar ESX-1-dependent increases in phagosomal damage, showing that this was not the case and suggesting that mTOR-deficient macrophages were sensitized to ESX-1-mediated mitochondrial rather than phagosomal damage (Figure 6A and 6B).

ESX-1-mitochondrial damage in mTOR-deficient macrophages could be indirect or direct. In the indirect case, ESX-1 would permeabilize the phagosome allowing either host lysosomal factors or a different mycobacterial determinant to damage the mitochondria. In the direct case, ESX-1 would first damage phagosomes, which would allow it to contact mitochondria and directly damage them. To distinguish between the two, we treated THP-1 cells with prazosin, a drug that permeabilizes endo-lysosomal compartments in myeloid cells (Kozik et al., 2020). By 7 hours of treatment, prazosin had caused extensive endo-lysosomal damage in uninfected control and mTOR-deficient macrophages as evidenced by galectin-8 staining (Figure S4). In infected macrophages, prazosin caused similar increases in damaged wild-type and ESX-1-deficient mycobacterial phagosomes (Figure 6B). Moreover, the proportion of wildtype and ESX-1-mutant mycobacteria associated with damaged phagosomes was similar, showing that the prazosin-induced phagosomal permeabilization could equalize access of wildtype and ESX-1-deficient mycobacteria to the mitochondria (Figure 6C). Consistent with increasing bacterial exposure to mitochondria, prazosin increased cytochrome c release from wildtype-infected macrophages (Figure 6D). Prazosin-treated ESX-1 mutant-infected macrophages had a much smaller increase in cytochrome c release (33% of prazosin-treated wild-type), and significantly lower than in untreated wild-type macrophages (Figure 6D). These findings implicate ESX-1 in directly mediating mitochondrial damage after first damaging the phagosome to enable contact. The small increase in cytochrome c release in ESX-1-mutant infection suggest that additional mechanisms may also play a role, for instance PDIM. To corroborate these conclusions in vivo, we assessed bacterial cording in zebrafish with and without

prazosin treatment. As before, mTOR deficiency caused cording of wildtype but not ESX-1-deficient bacteria (Figure 6E). Prazosin treatment of mTOR mutants increased ESX-1-deficient cording only slightly, and significantly less than wildtype bacteria without prazosin (Figure 6E). These results show that ESX-1 possesses both phagosomal and mitochondrial damaging activity and that mTOR protects specifically against the latter. Our findings highlight the strength of mTOR as a “counter-virulence” factor against ESAT-6 and indicate that a small amount of ESAT-6 is sufficient to induce cytotoxicity in mTOR-deficient macrophages — even small numbers of severely growth — attenuated but ESX-1-competent mycobacteria rapidly induced cytotoxicity in them. Furthermore, mTOR-deficient macrophages tolerated infection with mycobacteria if their ESX-1 function was impaired. Furthermore, mTOR-deficient macrophages tolerated infection with mycobacteria so long as they did not express one specific virulence determinant.

DISCUSSION

The association of infections, including TB, with therapeutic mTOR blockade in organ transplantation and cancer is well recognized (Fijalkowska-Morawska et al., 2011; Garcia and Wu, 2016; Jeon et al., 2017; Ruiz-Camps and Aguilar-Company, 2021; Tsai et al., 2007). Since mTOR signaling in phagocytes, antigen-presenting cells, and T cells is critical for their development, homeostasis and/or function, it is likely that mTOR exerts its protective effects in TB through a myriad of mechanisms impacting innate and adaptive immune responses (Lachmandas et al., 2016; Powell et al., 2012; Sinclair *et al.*, 2017; Weichhart *et al.*, 2015). Our screen, undertaken in the sole context of innate immunity, uncovers an essential early protective role for mTOR well before adaptive immunity is generated. Still, our finding that mTOR confers innate resistance by enhancing macrophage survival would have been expected given that mTOR is known to support macrophage development and homeostasis and our previous findings that sustained myelopoiesis is critically important to maintain granuloma cellularity (Deng *et al.*, 2017; Karmaus *et al.*, 2017; Lee *et al.*, 2017; Mercalli *et al.*, 2006; Pagan *et al.*, 2015; Sinclair *et al.*, 2017; Weichhart *et al.*, 2015). The surprise is that mTOR deficiency results in the rapid depletion of infected macrophages through catastrophic mitochondrial damage caused specifically by ESAT-6/ESX-1, a major mycobacterial virulence determinant. A corollary of this finding is that mitochondrial metabolism represents a formidable armor against a potent mycobacterial mitotoxin. It is being increasingly appreciated that while intracellular microbes can exploit host cell metabolism for growth and pathogenesis, cellular metabolism, can in turn, use its

metabolic capabilities to avert microbial attack (Pernas, 2021). Our findings reveal the role of host metabolism in protection from a major infectious killer.

A major virulence attribute of ESX-1 is its ability to induce macrophage death even in wild-type (mTOR competent) macrophages (Groschel *et al.*, 2016; Ramakrishnan, 2012). Studies in cultured cells have attributed this death to apoptosis, pyroptosis or necrosis (Augenstreich *et al.*, 2017; Beckwith *et al.*, 2020; Behar et al., 2010; Srinivasan et al., 2014) and the one in vivo study, also in zebrafish larvae, finds that ESX-1 induces apoptosis of granuloma macrophages (Davis and Ramakrishnan, 2009). For all these forms of death, phagosomal damage is widely considered to be a pre-requisite step, which is now confirmed to be mediated by ESAT-6 (Bao *et al.*, 2021; Osman *et al.*, 2022; Simeone *et al.*, 2021; Srinivasan *et al.*, 2014; Zhang *et al.*, 2016). We show here that ESAT-6's ability to induce phagosomal damage is irrespective of whether the macrophage is mTOR-sufficient or -deficient, a finding that is important for its role in disease pathogenesis in normal hosts. Rather, we find that mTOR's specific role is in resistance against ESX-1-mediated *mitochondrial* damage. While Mtb can also damage the plasma membranes and mitochondrial membranes of mTOR-sufficient cells once it has accessed them through ESX-1-mediated phagosomal damage, the factors involved in those other forms of membrane damage remain unclear — studies have variably implicated ESAT-6, other ESX-1 substrates, non-ESX-1 mycobacterial products, excess lipoxins, and mROS (Beckwith *et al.*, 2020; Chen et al., 2008; Divangahi et al., 2009; Fine-Coulson et al., 2015; Lienard *et al.*, 2020; Sun et al., 2015; Wiens and Ernst, 2016). Here we show that ESX-1 directly induces mitochondrial damage in mTOR-deficient cells. However, we have not yet shown whether the

mitochondrial damage is through ESAT-6 or some other ESX-1 substrate. Similarly, we and others have shown that PDIM facilitates ESAT-6 mediated phagosomal damage, possibly by changing the characteristics of the mycobacterial surface, host membranes or both (Augenstreich *et al.*, 2017; Augenstreich et al., 2019; Cambier et al., 2020; Osman *et al.*, 2020; Simeone *et al.*, 2021). In this work, we show that PDIM is essential for the mitochondrial damage and death in mTOR deficiency but whether this effect is solely by causing phagosomal damage or whether it additionally works with ESX-1/ESAT-6 to damage mitochondrial membranes remains a question.

How does ESX-1 damage mitochondria? Mm and Mtb phagosomes frequently fuse to lysosomes, and contacts between lysosomes and mitochondria are proposed to facilitate metabolic exchanges between these organelles (Armstrong and Hart, 1971; Barker et al., 1997; Clemens and Horwitz, 1995; Harris et al., 2008; Levitte *et al.*, 2016; Wong et al., 2018). The idea that mycobacterial phagolysosomes influence mitochondrial function is reinforced by the finding that mitochondria aggregate around these structures and undergo morphological changes (Jamwal et al., 2013; Mohareer et al., 2020). Given that direct contact is required for ESX-1 permeabilization of host membranes (Conrad *et al.*, 2017), we speculate that ESAT-6 or a different secreted ESX-1 substrate might specifically damage mitochondria that are in direct contact with permeabilized phagosomes through sequential disruption of the outer and inner mitochondrial membranes (Figure 7). Even at low levels of infection, damage to the already metabolically-impaired mitochondria of mTOR-deficient macrophages would further atrophy mitochondrial energetic metabolism, thereby promoting lethal reduction in cellular energy reserves. This additional drop in energetic output would be expected

to further impair the cell's ability to repair or replace damaged organelles, including mitochondria.

Our findings provide insight into the adaptive metabolic changes that occur upon mycobacterial infection. Stimulation of cultured macrophages with bacterial Toll-like receptor (TLR) ligands like lipopolysaccharide (LPS) under normoxic conditions induces a metabolic switch from mitochondrial OXPHOS to glycolysis through activation of mTORC1 (O'Neill and Pearce, 2016; Weichhart *et al.*, 2015). This switch enables macrophages to elaborate antimicrobial responses that depend on cataplerosis of Krebs cycle intermediates (Ryan and O'Neill, 2020). However, it is not clear to what extent Mtb-infected macrophages undergo this glycolytic switch. Some studies find that Mtb infection boosts glycolysis while others find that it represses it (Braverman et al., 2016; Cumming et al., 2018; Gleeson et al., 2016; Huang et al., 2018; Lachmandas *et al.*, 2016; Shi et al., 2015). These conflicting findings may reflect the muted metabolic response to mycobacterial infection in comparison to LPS, perhaps because they largely evade TLR recognition (Cambier *et al.*, 2014a; Cambier *et al.*, 2014b; Hinman et al., 2021; Holscher et al., 2008; Mayer-Barber et al., 2010). Indeed, in vivo, we have shown that both Mm- and Mtb-infected macrophages exhibit small increases in mitochondrial respiration early on (Roca, 2022). Our current work shows that these and the resultant increases in ATP, which require mTORC1 signaling, though small, constitute critical metabolic adaptations to cope with mycobacterial invasion. Importantly, these metabolic adaptations are required only to resist ESX-1-induced mitochondrial damage — mycobacteria not expressing ESX-1 are well tolerated by macrophages lacking mTOR.

While we cannot rule out adaptive glycolytic shifts later in infection, our data are consistent with mTORC1's role in resistance immediately upon mycobacterial invasion stemming from the boost in OXPHOS that comes from its stimulation of glycolysis (Weichhart *et al.*, 2015). Indeed, our finding that inhibition of pyruvate import into mitochondria confers susceptibility highlights that glycolysis alone cannot compensate for the deficits in mitochondrial metabolism caused by mTOR deficiency. mTOR regulated biosynthetic processes may rapidly replace or repair damaged mitochondria, consistent with the known roles of mTORC1 signaling mitochondrial physiology (Cunningham *et al.*, 2007; Liu and Sabatini, 2020; Morita *et al.*, 2013; Morita et al., 2017; Rambold and Pearce, 2018; Schieke *et al.*, 2006). Alternatively, these same mTOR functions may ensure that there is a sufficient pool of functional mitochondria to maintain the cell's energetic demands even when some mitochondria are damaged by ESX-1. Furthermore, as macrophages need OXPHOS to activate antigen-specific T cells and to respond to interferon-γ (Kiritsy et al., 2021), maintaining mitochondrial function in Mtb-infected macrophages may be a prerequisite for effective T cell-mediated immunity in the granuloma.

Induction of macrophage death is a major pathogenic mechanism used by mycobacteria. Early on, apoptotic death of infected macrophages can promote intercellular mycobacterial spread and thereby expansion of their numbers in early granulomas (Davis *et al.*, 2002; Ramakrishnan, 2012). ESX-1/ESAT-6 are implicated in this apoptotic death as well as other forms of programmed cell death like pyroptosis and necrosis, which involve plasma membrane damage (Augenstreich *et al.*, 2017; Beckwith *et al.*, 2020; Behar *et al.*, 2010; Divangahi *et al.*, 2009; Srinivasan *et al.*, 2014). ESX-1 is

also implicated in the type-1 interferon (T1-IFN)-mediated cytotoxicity induced by Mtb (Manzanillo et al., 2012; Mayer-Barber et al., 2014; Moreira-Teixeira et al., 2018; Stanley et al., 2007; Zhang et al., 2021). While this form of death does involve mitochondria — ESX-1-promoted mitochondrial DNA release stimulates cytosolic DNA-sensing pathways (Hopfner and Hornung, 2020; Lienard *et al.*, 2020; Wiens and Ernst, 2016) — its effects on the metabolism of both Mtb-infected and uninfected (bystander) macrophages suggest a distinct cytotoxicity mechanism. T1-IFNs produced in response to *M. tuberculosis* infection repress glycolysis and OXPHOS in both infected and uninfected (bystander) macrophages and induce pathogenic levels of mROS in the infected cells (Cumming *et al.*, 2018; Olson et al., 2021; Wiens and Ernst, 2016). We show that if mTOR is lacking, the above modes of ESX-1-mediated death become irrelevant, because the cells die more rapidly from the inability to boost mitochondrial metabolism in response to infection. Thus, the other forms of ESX-1-mediated death — ultimately also mediated by its membranolytic activity — represent “workarounds” in mycobacterium’s pathogenic strategy.

TB is notorious for killing far more people over the millenia than any other infectious agent (Paulson, 2013). Yet, our recent epidemiological analyses show that most individuals clear Mtb infection through a combination of innate and adaptive immunity (Behr *et al.*, 2018; 2019; Behr *et al.*, 2021). Understanding the immune correlates of protection in the many is an active focus of TB researchers. Our work finds that tapping into mTOR-regulated homeostatic metabolic pathways constitutes a major host defense strategy. Curiously, these pathways protect against a specific mycobacterial virulence determinant. Indeed, identifying mTOR as a “counter-virulence”

factor against mycobacterium ESX-1 exemplifies TB as a paradigm of the host-pathogen interaction, where the evolutionary survival of both host and pathogen are ensured (Cambier *et al.*, 2014a). mTOR buys the host time to call in other defenses that can clear infection much of the time, while the success of the ESX-1 virulence mechanism in the minority of infected individuals has assured Mtb survival over the millennia.

ACKNOWLEDGEMENTS

We thank M. Behr, P. Edelstein, M. Murphy and F. Roca for discussions; M. Eisenberg-Bord and N. Yamaguchi for manuscript review; K. Takaki for parabiosis instruction; C. Hale for providing access to Seahorse XFp analyzer and advice on experimental design; J. Ray for assistance mapping *mtor*^{fh178}; R. Berg, L. Hernández, S. Levitte, and J. Zimmermann for assistance with early characterization of *mtor*^{fh178}; H. Boyd, B. Brockley, C. Dooley, S. McGuinan, R. Santhakumar, I. Smallwood, and R. White for technical and logistical assistance with genetic screens; J. Cameron, N. Goodwin, R. Foster, and the University of Cambridge aquatics facility staff for zebrafish husbandry; the LMB's flow cytometry core facility and the NIHR Cambridge BRC Cell Phenotyping Hub for equipment access, and the LMB's media service for preparation of bacterial and tissue culture reagents. This work was supported by the National Institutes of Health (T32-AI055396, A.J.P. and MERIT award R37-AI054503 and Director's Pioneer Award DP1MH099901, L.R.), a Wellcome Trust Principal Research Fellowship (223103/Z/21/Z; L.R.), the Max Planck Society (E.L.P.), and the Liebnietz Prize (E.L.P).

AUTHOR CONTRIBUTIONS

A.J.P., C.B.M., D.M.T., and L.R. conceived the project. A.J.P., L.J.L., J.E.-H., C.B.M., D.M.T., E.M.B.-N., E.L.P. and L.R. designed experiments and analyzed data. A.J.P. and L.J.L. performed zebrafish experiments. D.M.T. isolated and mapped *mtor*^{fh178}. A.J.P. conducted cell culture experiments. J.E.-H. performed and analyzed LC/MS. C.B.M. and E.M.B.-N. provided chemically-mutagenized zebrafish lines. E.L.P. suggested and supervised metabolomics experiments and advised on the experimental design and interpretation of metabolic experiments. A.J.P. and L.R. wrote the manuscript and got input from the other authors.

DECLARATION OF INTERESTS

E.L.P. is a scientific advisory board member of ImmunoMet and a founder of Rheos Medicines. For the purpose of open access, the authors have applied a CC BY public copyright license to any Author Accepted Manuscript version arising from this submission. This work is licensed under a Creative Commons Attribution 4.0 International License.

FIGURE LEGENDS

Figure 1. mTORC1-deficient Zebrafish Are Hypersusceptible to Mm Infection.

(A) Illustration of hindbrain ventricle (hbv) and caudal vein (cv) injection routes used in this study.

Larvae were infected with ~150 Mm expressing tdTomato (B, C, E - J) or tdKatushka2 (D) fluorescent proteins via the caudal vein two days post fertilization (dpf).

(B) Overlaid micrographs of widefield mycobacterial fluorescence (Mm, red) and brightfield in *mtor*$^{fh178/fh178}$ or wildtype siblings (*mtor*$^{+/+}$) four days post infection (dpi).

(C) Quantification of bacterial fluorescence (fluorescent pixel counts, FPC) in animals from *mtor*$^{fh178/+}$ incross 4 dpi. Symbols represent individual animals. Horizontal lines indicate mean values.

(D) Confocal micrographs of *mtor*$^{fh178/fh178}$ and a wildtype sibling expressing *Tg(mpeg1:YFP)* 4 dpi showing a granuloma in the wildtype animal and mycobacterial cording in the *mtor*$^{fh178/fh178}$ animal. Mm (magenta) and macrophages (green) are shown. Arrowheads indicate intracellular Mm. Bracket indicates extracellular Mm with corded morphology.

Mycobacterial cording in animals from (E) *mtor*$^{fh178/+}$ incross, (F) *mtor*$^{sa16755/+}$ incross, (G) *mtor*$^{fh178/+}$ x *mtor*$^{sa16755/+}$ complementation cross, and (H) *rptor*$^{sa11537/+}$ incross at 4 dpi, and (I) *rictora*$^{sa15967/+}$*; rictorb*$^{sa18403/+}$ double heterozygote incross and (J) wildtype animals treated with torin1 (400 nM), rapamycin (400 nM), or 0.5% DMSO (vehicle control) 5 dpi. (E - J) Numbers within columns indicate animals per group.

Scale bars, (B) 300 μm and (D) 25 μm. Statistical analyses, (C) one-way ANOVA with Tukey's post-test and (E - J) Fisher's exact test. ****$p < 0.0001$. Data shown are representative of two or more independent experiments.

Figure 2. mTOR Deficiency Impairs Macrophage Development and Survival and Sensitizes Infected Macrophages to Mycobacterium-induced Cytotoxicity.

Zebrafish larvae were infected with Mm expressing BFP2 (A, E, I - N), mWasabi (C, D) or tdKatushka2 (F - H) fluorescent proteins via the hindbrain ventricle (A) or the caudal vein (B - N) 2 dpf.

(A) Confocal micrographs showing serial imaging of granulomas in *Tg(mfap4:tdTomato-CAAX)* zebrafish treated with Rapamycin or DMSO. Mm (cyan) and macrophages (red) are shown.

(B) (Top) Illustration of macrophage counting region (shaded light blue). (Bottom) Numbers of macrophages in Mm- and mock-infected Raptor mutants and siblings expressing *Tg(mpeg1:tdTomato)*. Symbols indicate mean values for each group and error bars show Standard Error of the Mean (S.E.M.).

(C) Percentage of Raptor mutants and siblings showing mycobacterial cording.

(D) Time-lapse confocal micrographs capturing the death of macrophage infected with a single bacterium in an *mtor*$^{sa16755/sa16755}$*; Tg(mfap4:tdTomato-CAAX); Tg(ubb:secA5-YFP)* animal 2 dpi. Mm (blue), secreted annexin V-YFP (green), and macrophage (magenta) are shown. Arrowheads indicate annexin V-decorated blebs. See Movie S1.

(E - G) 6-hr time-lapse confocal microscopy of *mtor*$^{fh178/fh178}$ and mTOR-sufficient siblings expressing *Tg(mpeg1:YFP)* 2 dpi. See Movie S2.

(E) Absolute numbers of infected macrophages in the imaged field.

(F) Percentage of dying macrophages in the imaged field.

(G) Relative mycobacterial burdens in dying macrophages of *mtor*$^{-/-}$ and mTOR-sufficient fish. Bacterial volumes were normalized to values obtained from dying cells in mTOR-sufficient controls for each imaging run.

(H) Widefield micrograph of parabiotic zebrafish comprised of conjoined wild-type *Tg(mpeg1:tdTomato)* and *mtor*$^{fh178/fh178}$*; Tg(mpeg1:YFP)* embryos 4 dpi.

(I) Macrophage counts (normalized to each genotype's initial counts) in the WT body (top) and *mtor*$^{-/-}$ body (bottom) of WT - *mtor*$^{-/-}$ parabiont.

(J) Maximum intensity projections of infections in the WT body (top) and *mtor*$^{-/-}$ body (bottom) of a WT - *mtor*$^{-/-}$ parabiont 4 dpi.

(K) Widefield micrograph of wild-type *Tg(mpeg1:tdTomato)* and *mtor*$^{fh178/+}$*; Tg(mpeg1:YFP)* parabiont 4 dpi.

(L) Macrophage counts (normalized to each genotype's initial counts) in the WT body (top) and *mtor*$^{+/-}$ body (bottom) of WT - *mtor*$^{+/-}$ parabiont.

(M) Maximum intensity projections of infections in the WT body (top) and *mtor*$^{+/-}$ body (bottom) of a WT - *mtor*$^{+/-}$ parabiont 4 dpi.

Scale bars, (A) 25 µm, (D) 10 µm, (H, K) 400 µm, and (J, M) 50 µm. Statistical analyses, (E - G) two-tailed, unpaired Student's *t* test. $^{**}p < 0.01$. Time lapse data were pooled from five (E and F) or three (G) independent experiments.

Figure 3. mTOR Deficiency Impairs Mitochondrial Metabolism in Macrophages and Facilitates Mycobacterium-induced Mitochondrial Damage.

(A, B) *mtor*$^{fh178/fh178}$ and mTOR-sufficient siblings expressing *Tg(mpeg1:YFP)* were infected intravenously with Mm expressing BFP2 on 2 dpf and injected intravenously with MitoTracker Red CMH_2-Xros one day later.

(A) Confocal micrograph illustrating mROS detection in an infected animal. Macrophages (green), Mm (blue), and mROS (magenta) are shown. Arrowheads indicate mROS-producing infected cells. Scale bar, 20 μm.

(B) Quantification of MitoTracker Red CMH_2-Xros mean fluorescence intensity (MFI) in infected and uninfected macrophages of *mtor*$^{-/-}$ animals and siblings at 1 dpi. Symbols represent individual macrophages. Horizontal lines indicate mean values.

THP-1 macrophages were treated with torin1 or DMSO and infected with (C, D, G, H) tdTomato- (E, F) or mWasabi-expressing Mm at a multiplicity of infection (MOI) of 1 (C - F) or 3 (G, H).

(C) Flow cytometry plots of cell viability 2 dpi. Percentages of non-viable cells (FVD eFluor 660^{+}) in the infected and uninfected subpopulations are shown.

(D) Quantification of non-viable cells. Symbols represent values from individual wells, and bars indicate mean values.

(E) Flow cytometry histograms of TMRE fluorescence 1dpi.

(F) TMRE geometric mean fluorescence intensities (GeoMFI) 1 dpi. Symbols represent values from individual wells, and bars indicate mean values.

(G) Flow cytometry histograms of cytochrome c (cyt c) fluorescence in infected viable cells (FVD eFluor 660^{-}) 7 hours post infection (7 hpi). Gate indicates population of cells that have released cyt c.

(H) Quantification of cyt c^{low} cells 7 hpi.

Statistical analyses, (B) one-way or (D, H) two-way ANOVA with Tukey's post-test. *$p < 0.05$, **$p < 0.01$, ***$p < 0.001$, and ****$p < 0.0001$. (A, B) Data are representative of two experiments. See also Figure S1.

Figure 4. Glycolysis Inhibition Impairs Mitochondrial Metabolism and Sensitizes Infected Macrophages to Mycobacterium-induced Cytotoxicity.

THP-1 macrophages treated with torin1 (400 nM), 2-deoxy-D-glucose (2DG, 5 mM) or DMSO were infected with Mm expressing (A) BFP2 or (B, K) tdTomato (MOI = 1).

(A) TMRE GeoMFI 1 dpi.

(B, C) Percentage of non-viable cells (FVD eFluor 660^{+}) 1 dpi.

(D - H, J) Zebrafish were infected with ~150 fluorescent Mm via the caudal vein.

(D) 5 dpi macrophage numbers in the body of mock- or Mm-infected *Tg(mpeg1:YFP)* zebrafish fish treated with 50 mM 2DG or 0.5% DMSO.

(E, F) 6-hr time-lapse confocal microscopy of *Tg(mpeg1:YFP)* 3 dpi. (D) Absolute numbers of infected macrophages in the imaged field. (E) Percentage of dying infected macrophages in the imaged field. See Movie S3.

(G) Mycobacterial cording in 2DG- and DMSO-treated wildtype animals 5 dpi.

(H) Mycobacterial cording in wildtype animals treated with UK5099 (10 μM) or 0.5% DMSO 5dpi.

(I) Glucose-6 phosphate dehydrogenase (G6PD) activity in 5 dpf animals from *g6pd*$^{sa24272/+}$ incross.

(J) Mycobacterial cording in animals from *g6pd*$^{sa24272/+}$ incross 5 dpi.

(K) ATP concentration per well containing 10^6 THP-1 cells 1 dpi.

Symbols represent values from individual (A- C, K) wells or (D - J) animals. (A - C, I, K) Bars and (D - F) horizontal lines indicate mean values. (G, H, J) Numbers within columns indicate animals per group. Statistical analyses, one-way ANOVA with (A - C) Sidak or (D, I) Tukey post-tests, (E, F) unpaired Student's *t* test, or (G, H, J) Fisher's exact test. *$p < 0.05$, **$p < 0.01$, ***$p < 0.001$, and ****$p < 0.0001$. (E, F) Time-lapse data were pooled from two independent experiments. Data are representative of (A, G, H) two independent experiments. See also Figure S2.

Figure 5. Deficiencies in mTOR, Glycolysis, and Mitochondrial Import of Pyruvate Sensitize Macrophages to Mycobacterial ESAT-6-dependent Cytotoxicity.

(A) Cytochrome c release 7 hpi in THP-1 macrophages infected with BFP2-expressing WT or Δ*ESX-1* Mm at MOI = 3.

(B) Percentage of dying cells (SYTOX Green$^+$) during 4-hr time-lapse at 1 dpi with tdTomato-expressing WT or Δ*ESX-1* Mm at MOI = 1. Values from uninfected (U) and infected (I) cells from the same fields are shown. See Movie S4.

(C - H) Zebrafish were infected with dose-matched inocula of tdTomato-expressing *Mm* of the indicated strains via the caudal vein.

(C) Percentage of dying infected macrophages in 6-hr time-lapse confocal microscopy of *mtor*$^{fh178/fh178}$ and *mtor*-sufficient siblings expressing *Tg(mpeg1:YFP)* 2 dpi. See Movie S5.

(D) Mycobacterial cording in *mtor*$^{fh178/fh178}$ animals and *mtor*-sufficient siblings 4 dpi.

(E, F) Mycobacterial cording in wildtype zebrafish treated with 2DG, UK5099, or DMSO 5 dpi.

(G) Mycobacterial cording in *mtor*$^{sa16755/sa16755}$ animals and *mtor*-sufficient siblings 4 dpi. See also Figure S3.

(H) Mycobacterial cording in *mtor*$^{fh178/fh178}$ animals and *mtor*-sufficient siblings 4 dpi with *ΔesxA* Mm complemented with wild-type or point mutant Mtb *esxA*.

Symbols represent values from individual (A) wells, (B) imaging fields, or (C) animals. (A, B) Bars and (C) horizontal lines indicate mean values. (D - H) Numbers within columns indicate animals per group. Statistical analyses, (A - C) one-way ANOVA with Sidak's post-test or (D - H) Fisher's exact test. *$p < 0.05$, **$p < 0.01$, ***$p < 0.001$, and ****$p < 0.0001$. (B, D) Data are representative of two experiments. Zebrafish time-lapse data were pooled from three experiments.

Figure 6. ESX-1 Mediates Mitochondrial Damage in mTOR-deficient Macrophages Downstream of Its Involvement in Phagosomal Permeabilization.

(A - E) Torin1- and DMSO-treated THP-1 macrophages were infected with tdTomato-expressing WT or Δ*ESX-1* Mm at MOI = 3 and treated with prazosin (PRZ, 20 μM) for 7 hrs. See also Figure S4.

(A) Confocal micrographs of Galectin-8 (GAL8) immunofluorescence (green) and Mm fluorescence (magenta) in THP-1 macrophages 7 hpi. GAL8 foci associated with

Mm (filled arrowheads) or not associated with Mm (open arrowheads) are shown. Scale bar, 20 μm.

(B) Percentage of macrophages with GAL8-associated Mm foci.

(C) Percentage of Mm volume associated with GAL8 foci 7 hpi.

(D) Percentage of cells that have released cytochrome c 7 hpi.

(E) *mtor*$^{sa16755/sa16755}$ fish and *mtor*-sufficient siblings were infected with ~90 fluorescent Mm via the hindbrain ventricle on 2 dpf. On 1 and 2 dpi, fish were injected with ~3 nL of 300 μM PRZ or 1% DMSO into the hindbrain ventricle. Graph indicates the percentage of animals with mycobacterial cording 3 dpi.

Symbols represent values from individual (B, C) imaging fields or (D) individual wells. (B, C) Horizontal lines and (D) bars indicate mean values. (E) Numbers within columns indicate animals per group. Statistical analyses, (B, D) one-way ANOVA with Sidak's post-test or (E) Fisher's exact test. *$p < 0.05$, **$p < 0.01$, ***$p < 0.001$, and ****$p < 0.0001$.

Figure 7. Cartoon Model Depicting the Role of mTOR-associated Mitochondrial Energy Metabolism in Protection from Mycobacterial ESAT-6-induced Mitochondrial Damage and Cytotoxicity.

MATERIALS AND METHODS

RESOURCE AVAILABILITY

Additional information and requests for resources and reagents should be directed to and will be fulfilled by the Lead Contact, Lalita Ramakrishnan (lalitar@mrc-lmb.cam.ac.uk).

EXPERIMENTAL MODEL AND SUBJECT DETAILS

Ethics Statement

Zebrafish husbandry and experiments were carried out in compliance with guidelines from the UK Home Office and the US Public Health Service Policy on Human Care and Use of Laboratory Larvae using protocols approved by the Animal Welfare and Ethical Review Body of the University of Cambridge and the Institutional Animal Care and Use Committee of the University of Washington, respectively.

Zebrafish Husbandry and Infections

Zebrafish of the wild-type AB strain (Zebrafish International Resource Center, ZIRC), TL strain (ZIRC), or of mixed AB/TL backgrounds were used in experiments (Table S2). The *Tg(mpeg1:YFP)*^{w200}*, Tg(mpeg1:Brainbow)*^{w201} (described as *mpeg1:tdTomato*), *Tg(mfap4:tdTomato-CAAX)*^{xt6}*, Tg(CMV:EGFP-map1lc3b)*^{zf155}, and *Tg(ubb:secA5-YFP)*^{cu34} (this work) fluorescent reporter lines were maintained in the AB strain (He et al., 2009; Pagan *et al.*, 2015; Roca and Ramakrishnan, 2013; Walton et al., 2015) (Table S2). The *mtor*^{fh178} mutant line (this work) was generated and maintained in the

AB strain. The *mtor*^{sa16755}, *rptor*^{sa11537}, *rictora*^{sa15967}, *rictorb*^{sa18403}, *atg12*^{sa42684}, and *g6pd*^{sa24272} mutant lines (Wellcome Trust Sanger Institute) (Kettleborough *et al.*, 2013) were generated in the TL strain and maintained in either the TL strain (*rictora*^{sa15967}, *rictorb*^{sa18403}, and *g6pd*^{sa24272}) or mixed AB/TL backgrounds (*mtor*^{sa16755}, *rptor*^{sa11537}, and *atg12*^{sa42684}) (Table S2). Zebrafish of the WIK strain (ZIRC) were used to map *mtor*^{fh178}. Zebrafish were maintained in buffered reverse osmotic water systems under a 14-hr light/10-hr dark cycle. Zebrafish larvae were fed paramecia twice daily, while juvenile and adult zebrafish were fed at least twice a day with dry food and brine shrimp. Zebrafish embryos were collected and cultured in reverse osmosis water containing 0.18g/L Instant Ocean Salt supplemented with 0.25μg/mL methylene blue at 28.5°C. On 1 dpf, embryos to be used in experiments were transferred to 0.5x E2 medium (7.5mM NaCl, 0.25mM KCl, 0.5mM $MgSO_4$, 0.075mM KH_2PO_4, 0.025mM Na_2HPO_4, 0.5mM $CaCl_2$, and 0.35mM $NaHCO_3$) supplemented with 0.003% PTU (1-phenyl-2-thiourea, Sigma) to inhibit melanin synthesis.

For infections, 2 dpf larvae of undetermined sex (due to early developmental stage) were dechorionated manually or with ≤0.5mg/mL pronase (Sigma-Aldrich) and then anesthetized with fish water containing 0.025% tricaine (Sigma-Aldrich). Larvae were injected via the caudal vein or the hindbrain ventricle using single-cell suspensions of Mm of known titer to deliver ~100 - 250 bacteria per 3 - 5nL injection as previously described (Takaki et al., 2013). Phenol red sodium salt (≤ 1% w/v diluted in PBS, Sigma-Aldrich) was used as an injection tracer. Inoculums were confirmed by injecting onto Middlebrook 7H10 agar plates (supplemented with oleic acid, albumin, dextrose, and Tween-80 plus hygromycin B or kanamycin, as appropriate. For experiments with

mutant lines, wild-type and heterozygous siblings were used as comparators, animals were genotyped after data acquisition. In experiments involving drug treatments, infected animals were randomly assigned to treatment groups. Unless indicated, treatments (Table S2) were initiated immediately after infection via soaking, and drug exposure was maintained until the experimental endpoint. UK5099 (Cambridge Bioscience) was changed daily.

THP-1 Macrophage Culture and Infections

Monocytic human THP-1 cells (ATCC) were grown at 37°C, 5% CO_2 in RPMI medium (Sigma-Aldrich) supplemented with 10% FBS (Gibco), L-glutamine (Gibco), Penicillin, and Streptomycin (complete RPMI) (Table S2). To differentiate THP-1 cells into macrophages, cells were seeded at 5 x 10^5 cells/mL in flat-bottomed tissue culture plates (2.5 x 10^5 cells/well of 24-well plate) and stimulated with 100nM PMA Phorbol 12-myristate 13-acetate (Sigma-Aldrich) for two days. The resulting adherent cells were then washed with complete RPMI and rested for two days prior to infection. For microscopy experiments, cells were plated on optical bottom plates (Perkin Elmer or MatTek). Cells were pre-incubated overnight with pharmacological compounds or matching concentrations of vehicle (≤0.5% DMSO). On the infection day, cells were washed with antibiotic-free complete RPMI and infected with single-cell suspensions of Mm or Mtb for five hours in a 33°C, 5% CO_2 incubator (for Mm) and 37°C, 5% CO_2 incubator (for Mtb). After infection, cells were washed with antibiotic-free complete RPMI supplemented with the corresponding pharmacological compounds and returned to the appropriate incubators. For experiments with the leucine and pantothenate

double auxotroph *ΔleuDΔpanCD* Mtb, complete RMPI was also supplemented with 0.05 mg/mL L-leucine and 0.024 mg/mL calcium pantothenate (Sigma-Aldrich). Multiplicity of infection was determined by calculating the number of mycobacterial colony forming units (CFU) per cells plated in each well.

METHOD DETAILS

Bacterial Strains

M. marinum M strain (ATCC #BAA-535) and its mutant derivatives *ΔESX-1*, *ΔmmpL7*, *Δerp*, *marP::tn*, and *ΔesxA* expressing BFP2, mWasabi, tdTomato, or tdKatushka2 under the control of the *msp12* promoter (Cambier *et al.*, 2014b; Cosma *et al.*, 2006; Levitte *et al.*, 2016; Osman *et al.*, 2022; Takaki *et al.*, 2013) were grown at 33°C under hygromycin B (Cambridge Bioscience) or kanamycin (Sigma-Aldrich) selection in Middlebrook 7H9 medium (BD Difco) supplemented with oleic acid, albumin, dextrose, and Tween-80 (Sigma-Aldrich) (Takaki *et al.*, 2013) (Table S2). *M. tuberculosis ΔleuDΔpanCD* mc^2 6206 expressing *msp12:tdTomato* was grown at 37°C under hygromycin B and kanamycin selection in Middlebrook 7H9 medium supplemented with oleic acid, albumin, dextrose, Tween-80, catalase, and 0.05 mg/mL L-leucine and 0.024 mg/mL calcium pantothenate (Sigma-Aldrich) (Roca *et al.*, 2019; Sampson *et al.*, 2011).

Zebrafish Genotyping

DNA from adult fin clips or whole larvae was extracted using the HotSHOT method (Truett et al., 2000). Animals were genotyped by High Resolution Melt Analysis (HRMA)

of PCR products (Garritano et al., 2009) or by Kompetitive Allele-Specific PCR (KASP) assay (LGC Biosearch) (He et al., 2014) in a CFX Connect thermocycler (BioRad) (Table S2). DNA from 2DG-treated animals was purified with AMPure XP beads (Beckman Coulter) according to the manufacturer's instructions prior to PCR.

Mapping of *mtor*^{fh178}

Zebrafish carrying the *fh178* allele were outcrossed to the WIK strain for mapping as previously described (Tobin *et al.*, 2010). *fh178* was mapped to chromosome 8 initially between the markers z7370 and z14670. Further mapping defined a critical two-gene interval that included *mtor* and *qars1* to the right of a single nucleotide polymorphism in the 3' end of *angptl7* (1 recombination in 302 meioses) and to the left of a polymorphism in intron 2 of *ogg1* (2 recombinations in 300 meioses). Sequencing of cDNAs isolated from mutants and wild-type animals in the critical region identified a stop codon in exon 24 of *mtor* in the mutant but not wild-type animals. This mutation segregated absolutely with the *fh178* mutants (no recombinants).

Creation of *Tg(ubb:secA5-YFP)*^{cu34}

The Tol2 *ubb:secA5-YFP* plasmid was assembled from PCR-amplified fragments of pDestTol2pA2_ubi:EGFP (RRID: Addgene 27323) (Mosimann et al., 2011) and pBH-UAS-secA5-YFP (RRID: Addgene 32359) (van Ham et al., 2010) the Gibson Cloning kit (New England Biolabs) (Table S2). Correct plasmid assembly was confirmed by diagnostic PCR of joined segments and by Sanger sequencing. Tol2 transposase (RRID: Addgene 51818) (Khattak et al., 2014) was in vitro transcribed with the T7

mMessage/mMachine kit (ThermoFisher) according to the manufacturer's instructions (Table S2). Tol2 *ubb:secA5-YFP* plasmid and transposase mRNA were co-injected into one-cell embryos of the wild-type AB strain as previously described (Suster et al., 2011). G_0 larvae expressing the transgene were identified by fluorescence microscopy and raised to adulthood. Potential founders were identified through pairwise crosses of G_0 adults and non-transgenic AB fish. A single F_1 transgenic animal was used to establish the line.

Parabiosis

Parabiosis of zebrafish embryos was performed as previously described (Demy et al., 2013). Briefly, blastulae derived from synchronized *mtor*$^{fh178/+}$*; Tg(mpeg1:YFP)*^{w200} and *Tg(mpeg1:tdTomato)* incrosses were manually dechorionated, paired, scratched with an aluminum silicate microinjection needle, and allowed to fuse in high-calcium Ringer's solution (116 mM NaCl, 2.9 mM KCl, 10 mM $CaCl_2$, 5 mM HEPES, pH 7.2) supplemented with 50 U/mL penicillin and 50 U/mL streptomycin. Only parabiotic pairs fused at the head, devoid of gross morphological abnormalities, and sharing blood circulation were used in experiments. On 2 dpf, each parabiotic animal was infected via the caudal vein to ensure similar distribution of mycobacteria between the pair's caudal hematopoietic tissues. The bodies of each parabiotic pair were micro-dissected and individually genotyped after completion of the experiment.

Microscopy and Image Analyses

Widefield fluorescence microscopy was performed as previously described (Takaki *et al.*, 2013). Bacterial burdens were determined with a Nikon Eclipse Ti-E inverted microscope using a 4x objective and running a fluorescent pixel counts macro in ImageJ (National Institutes of Health) (Takaki *et al.*, 2013). Macrophages were counted manually with a Nikon Eclipse E600 upright microscope using a 20x objective. For serial imaging of individual zebrafish, larvae were housed individually in 96-well plates under standard husbandry conditions.

Laser scanning confocal microscopy was performed as described (Pagan *et al.*, 2015). Larvae were anesthetized in PTU-supplemented 0.5x E2 medium containing 0.025% tricaine and embedded in 2% low melt agarose (TopVision) on optical-bottom plates (MatTek). Imaging was performed with a Nikon A1R confocal microscope using 20x or 40x objectives and the galvano or resonant scanners. 0.9 - 2 μm optical sections were combined to generate 15 - 60 μm z stacks. For time-lapse microscopy of zebrafish larvae, imaging was done at 27°C using a microscope incubator (Okolab), using acquisition intervals of 2 - 5 minutes for 6 hours. For serial imaging of individual zebrafish, larvae were removed from the agarose using jeweler's forceps and housed individually under standard husbandry conditions. For time-lapse microscopy of Mm-infected THP-1 cells, samples were imaged at 33°C, 5% CO_2 in antibiotic-free, phenol-free complete RPMI containing 50 nM SYTOX Green nucleic acid stain (Invitrogen) for 4 hours.

The acquired images were processed using the denoising feature in the Elements software (Nikon). The surface rendering feature of Imaris (Bitplane) was used to quantify intramacrophage bacterial burdens and mROS levels; the number of acridine

orange foci in the midbrain and LC3 puncta in neuromasts, clusters of mechanosensory hair cells of the lateral line in fish; and the frequencies of galectin-8-associated Mm per imaging field (Thomas et al., 2015). The numbers of dying macrophages and macrophages with galectin-8-decorated Mm foci were counted manually.

Acridine Orange Staining

Zebrafish larvae were transferred to 1.5 mL microcentrifuge tubes and stained with 1 mL of 2.4μg/mL acridine orange in 0.5x E2 medium with PTU for 30 minutes with rotation and protected from light (Roca *et al.*, 2019). Stained larvae were then rinsed in 0.5x E2 medium with PTU and imaged by confocal microscopy.

MitoTracker Red CMXH_2-Xros Staining

Zebrafish larvae were injected with ~1 nL of 10 mM MitoTracker Red CMXH_2-Xros via the caudal vein immediately prior to imaging by confocal microscopy (Roca and Ramakrishnan, 2013).

Galectin-8 Immunostaining

The staining procedure was performed as previously described (Osman *et al.*, 2020). THP-1 cells were fixed in PFA solution (4% w/v paraformaldehyde in PBS) at room temperature (RT) for at least 30 minutes. Cells were then washed twice with PBS and incubated in permeabilization/block (PB) solution (0.1% Triton-X 100, 1% bovine serum albumin in PBS) for 30 minutes at RT, and subsequently stained with goat anti-human galectin-8 antibody (R&D Systems) diluted in PB solution overnight at 4°C. The

following day, cells were washed three times with PBS and stained with AlexaFluor488-conjugated donkey anti-goat IgG (ThermoFisher) in PB solution for one hour at RT. Cells were then washed three times with PBS and maintained in PBS for imaging by confocal microscopy.

Flow Cytometry

THP-1 macrophages were stained with Fixable Viability Dye (FVD) eFluor 660 (eBioscience), detached with Accutase (Sigma-Aldrich), and transferred to polystyrene FACS tubes (Sarstedt). Single-cell suspensions were washed with MACS buffer (0.5% bovine serum albumin, 2mM EDTA in PBS, ph7.2) at 290 x g for 5 minutes at 4°C, and in most cases, fixed in 4% PFA solution overnight at 4°C. The following day, samples were washed with and resuspended in MACS buffer. Data were acquired in LSRII or Fortessa flow cytometers (BD Biosciences) and analyzed in FlowJo 10 (TreeStar), gating on single-cell events.

TMRE Staining

THP-1 macrophages were incubated with 100 nM tetramethylrhodamine, ethyl ester (TMRE) (Abcam) for 20 minutes in a 37°C, 5% CO_2 incubator according to the manufacturer's instructions. Cells were then washed with complete RPMI media, stained with FVD eF660, and processed for flow cytometry as above but without fixation.

Cytochrome c Release Assay

The cytochrome c release assay was adapted from Lienard, et al. (Lienard *et al.*, 2020). 7 hours after infection with tdTomato-expressing Mm, cells were stained with Fixable Viability Dye (FVD) eFluor 660 (eBioscience), detached with Accutase (Sigma-Aldrich), transferred to polystyrene FACS tubes (Sarstedt), and washed first with ice-cold MACS buffer (0.5% bovine serum albumin, 2mM EDTA in PBS, ph7.2) and then ice-cold PBS by centrifugation at 290 x g for 5 minutes at 4°C. Cells were incubated in ice-cold permeabilization buffer (50 µg/mL digitonin, 100 mM KCl) for 5 minutes and immediately fixed in 4% PFA solution to stop the permeabilization reaction. Cells were then centrifuged as above and fixed overnight in 4% PFA solution at 4°C. Samples were analyzed by flow cytometry by gating on the viable, infected (FVD eFluor 660^{-} tdTomato^{+}) single-cell events.

ATP Quantification

ATP levels were quantified by fluorimetry in a CLARIOStar Plus (BMG Labtech) microplate reader using the ATP Assay Kit (Abcam) according to the manufacturer's instructions. 10^{6} THP-1 macrophages were analyzed per replicate.

Measurement of G6PD Activity

Individual 5 dpf larvae from an *g6pd*$^{sa24272/+}$ incross were lysed using Mammalian Cell Lysis Buffer (Abcam). A small amount of each lysate was used to genotype the larvae. G6PD activity in individual larvae was determined by fluorimetry in a CLARIOStar Plus (BMG Labtech) microplate reader using the G6PD Activity Assay Kit (Abcam) according to the manufacturer's instructions.

Metabolic Analyses

For metabolite quantification, THP-1 cells (2 x 10^6 cells/sample, four replicates/condition) were washed in ice-cold PBS, and metabolites were extracted with 150 μL extraction buffer (50:30:20, methanol:acetonitrile:water) cooled on dry ice for 30 minutes beforehand. Samples were then centrifuged at maximum speed for 10 minutes at °C to remove protein debris, and supernatants were stored at -80°C until acquisition. Liquid chromatography-mass spectrometry (LC-MS) was carried out using an Agilent 1290 Infinity II UHPLC in line with a Bruker Impact II QTOF operating in negative ion mode, as previously described (Edwards-Hicks et al., 2020). LC separation was performed on a Phenomenex Luna propylamine column (50 x 2 mm, 3 μm particles) using a solvent gradient of 100% buffer B (5 mM ammonium carbonate in 90% acetonitrile) to 90% buffer A (10 mM NH_4 in water). Flow rate was from 1000 to 750 μL/min. Autosampler temperature was 5°C, and injection volume was 2 μL. Metabolites were quantified using AssayR (Wills et al., 2017). The hierarchical clustering heatmap was generated in MetaboAnalyst 5.0 using Euclidean distance measure, the Ward clustering algorithm, and autoscale feature standarization (Pang et al., 2021).

Metabolic flux measurements were carried out with the Seahorse XFp Glycolytic Rate Assay and Cell Mito Stress Test kits (Agilent) according to the manufacturer's instructions. On the day of the assay, 4 x 10^4 differentiated THP-1 macrophages were seeded per well of the XFp cartridge, allowed to adhere for 2 hours in a 37°C, 5% CO_2 incubator, and then incubated with assay medium (XF DMEM medium with 10 mM glucose and 2 mM glutamine but without sodium pyruvate (Agilent)) for 45 - 60 minutes

in a non- CO_2 37°C incubator prior to data acquisition in a Seahorse XFp analyzer (Agilent).

Statistical Analyses

Statistical analyses were performed on Prism (GraphPad) with each statistical test and number of samples per group indicated in the corresponding figure legend. Not significant, $p > 0.05$; *$p < 0.05$; **$p < 0.01$; ***$p < 0.001$; ***$p < 0.0001$.

SUPPLEMENTARY FIGURES, TABLES, AND MOVIES

Figure S1. Inhibition of Autophagic Cell Death, Mitochondrial Apoptosis, or TNF-associated Necrosis Does Not Prevent Mycobacterium-induced Macrophage Death in mTOR-deficient Animals, Related to Figures 2 and 3.

(A) Confocal micrographs of LC3 clustering in neuromasts, clusters of mechanosensory cells of the fish lateral line, from *atg12*^{sa42684} incross fish expressing *Tg(CMV:lc3b-GFP)* 5 dpf. GFP fluorescence (top) and surface-rendered puncta (bottom) are shown. Scale bar, 10 μm.

(B) Number of LC3 puncta per neuromast.

(C) Mycobacterial cording in rapamycin- or DMSO-treated *atg12*^{sa42684} incross fish 5 dpi.

(D) Confocal micrographs of acridine orange (AO) staining (green) and surface-rendered puncta (magenta) in the midbrain of *casp9sa* incross fish 3 dpf. Scale bar, 50 μm.

(E) Number of AO puncta in the midbrain.

(F) Mycobacterial cording in rapamycin- or DMSO-treated *casp9*^{sa11164} incross fish 5 dpi.

(G) Illustration of necrosis pathway induced by mycobacterial infection plus excess TNF and pharmacological interventions tested.

(H, I) Mycobacterial cording in *mtor*$^{fh178/+}$ incross fish treated with (H) necrostatin-1, (I) nifedipine (5 μM), diltiazem (10 μM), or 0.5% DMSO 4 dpi.

Symbols represent individual (B) neuromasts or (E) animals. (B, E) Horizontal lines indicate mean values. (C, F, H, I) Numbers within columns indicate animals per group.

(B, E) one-way ANOVA with Tukey's post-test. *$p < 0.05$, ***$p < 0.001$, and ****$p < 0.0001$.

Figure S2. mTOR Inhibition Impairs Glycolysis and Mitochondrial Metabolism, Related to Figure 4.

(A) Metabolite profiles of THP-1 macrophages 1.5 days after treatment with torin1 (400nM), 2DG (5mM), or 0.5% DMSO. Heat map scale indicates relative $\log_2$ expression levels. See also Table S1.

(B) Diagram of Glycolytic Proton Efflux Rate (PER) assay.

(C) PER kinetics of THP-1 macrophages treated with torin1 or DMSO for 1.5 days.

(D) Basal and compensatory glycolytic PER.

(E) Diagram of Mitochondrial Oxygen Consumption Rate (OCR) assay.

(F) OCR kinetics of THP-1 macrophages treated with torin1 or DMSO for 1.5 days.

(G) Modular analysis of mitochondrial OCR.

(H) OCR kinetics of THP-1 macrophages treated with 2DG or DMSO.

(I) Modular analysis of mitochondrial OCR.

(J) Relative ATP levels in THP-1 macrophage cultures 1.5 days after treatment.

Symbols represent (B, C, E, F, H) mean values or (J) individual wells. (D, G, I, J) Bars indicate mean values. (D, G, I) Error bars depict Standard Deviation. (B, E) Arrows indicate the time of compound injection. Abbreviations: rotenone plus antimycin A (Rot + AA), 2DG, oligomycin (Oligo), carbonyl cyanide 4-(trifluoromethoxy)phenylhydrazone (FCCP), compensatory glycolysis (Comp), spare respiratory capacity (SRC).

Figure S3. Phagosome-damaging Capacity of ESX-1-competent Mycobacteria, Related to Figure 5.

(A) Confocal micrographs of Galectin-8 (GAL8) immunofluorescence (green) and Mm fluorescence (magenta) in THP-1 macrophages infected with the indicated Mm strains (MOI = 1) 1 dpi. The *ΔmmpL7* Mm strain is defective in PDIM transport to the myco-membrane. Bottom panels show area enclosed in dashed squares on top panels. Arrowheads indicate foci of GAL8-associated Mm. Scale bar, 25 μm.

(B) Percentage of macrophages with foci of GAL8-associated Mm. Symbols represent values from individual imaging fields. Horizontal bars indicate mean values. One-way ANOVA with Tukey's post-test, ****$p < 0.0001$.

Figure S4. Prazosin Damages Lysosomes of THP-1 Macrophages, Related to Figure 6.

Confocal micrographs of GAL8 immunofluorescence 7 hours after treatment with prazosin (PRZ, 20 μM) or 0.5% DMSO. Arrowheads indicate GAL8 puncta. Scale bar, 20 μm.

Table S1. Metabolite Profiles of THP-1 Macrophages Treated with Torin1, 2DG, or DMSO, Related to Figure S2.

Movie S1. Annexin V Labeling of a Dying, Mm-infected Macrophage in an mTOR Mutant Animal, Related to Figure 2. Time-lapse confocal microscopy of a dying, infected macrophage in an *mtor*$^{sa16755/sa16755}$*; Tg(mfap4:tdTomato-CAAX);*

Tg(ubib:secA5-YFP) animal 2 dpi. Mm (blue), secreted annexin V-YFP (green), and macrophage (magenta) are shown.

Movie S2. Death of Mm-infected Macrophages in mTOR Mutant Animals, Related to Figure 2. Time-lapse confocal microscopy of *mtor*$^{fh178/fh178}$ animals and mTOR-sufficient siblings expressing *Tg(mpeg1:YFP)*, 2 dpi. Mm (magenta) and macrophages (green) are shown. Arrows indicate dying infected macrophages.

Movie S3. Death of Mm-infected Macrophages in 2DG-treated Animals, Related to Figure 4. Time-lapse confocal microscopy of *Tg(mpeg1:YFP)* animals treated with 2DG or DMSO, 3 dpi. Mm (magenta) and macrophages (green) are shown. Arrows indicate dying infected macrophages.

Movie S4. Torin1-treated THP-1 Macrophages Tolerate *ΔESX-1* Infection, Related to Figure 5. Time-lapse confocal microscopy of THP-1 macrophage treated with torin1 or DMSO and infected with WT or Δ*ESX-1* Mm, 1 dpi. Mm (magenta) and SYTOX Green-labeled dying cells (green). Arrows indicate dying infected macrophages.

Movie S5. Macrophages of mTOR Mutant Animals Tolerate *ΔESX-1* Infection, Related to Figure 5. Time-lapse confocal microscopy of *mtor*$^{fh178/fh178}$ animals and mTOR-sufficient siblings expressing *Tg(mpeg1:YFP)* infected with WT or *ΔESX-1* Mm, 2 dpi. Mm (magenta) and macrophages (green) are shown. Arrows indicate dying infected macrophages.

REFERENCES

Amaral, E.P., Costa, D.L., Namasivayam, S., Riteau, N., Kamenyeva, O., Mittereder, L., Mayer-Barber, K.D., Andrade, B.B., and Sher, A. (2019). A major role for ferroptosis in Mycobacterium tuberculosis-induced cell death and tissue necrosis. J Exp Med *216*, 556-570. 10.1084/jem.20181776.

Armstrong, J.A., and Hart, P.D. (1971). Response of cultured macrophages to Mycobacterium tuberculosis, with observations on fusion of lysosomes with phagosomes. J Exp Med *134*, 713-740. 10.1084/jem.134.3.713.

Augenstreich, J., Arbues, A., Simeone, R., Haanappel, E., Wegener, A., Sayes, F., Le Chevalier, F., Chalut, C., Malaga, W., Guilhot, C., et al. (2017). ESX-1 and phthiocerol dimycocerosates of Mycobacterium tuberculosis act in concert to cause phagosomal rupture and host cell apoptosis. Cell Microbiol *19*. 10.1111/cmi.12726.

Augenstreich, J., Haanappel, E., Ferre, G., Czaplicki, G., Jolibois, F., Destainville, N., Guilhot, C., Milon, A., Astarie-Dequeker, C., and Chavent, M. (2019). The conical shape of DIM lipids promotes Mycobacterium tuberculosis infection of macrophages. Proc Natl Acad Sci U S A *116*, 25649-25658. 10.1073/pnas.1910368116.

Bao, Y., Wang, L., and Sun, J. (2021). A Small Protein but with Diverse Roles: A Review of EsxA in Mycobacterium-Host Interaction. Cells *10*. 10.3390/cells10071645.

Barker, L.P., George, K.M., Falkow, S., and Small, P.L. (1997). Differential trafficking of live and dead Mycobacterium marinum organisms in macrophages. Infect Immun *65*, 1497-1504. 10.1128/iai.65.4.1497-1504.1997.

Beckwith, K.S., Beckwith, M.S., Ullmann, S., Saetra, R.S., Kim, H., Marstad, A., Asberg, S.E., Strand, T.A., Haug, M., Niederweis, M., et al. (2020). Plasma membrane damage

causes NLRP3 activation and pyroptosis during Mycobacterium tuberculosis infection. Nature communications *11*, 2270. 10.1038/s41467-020-16143-6.

Behar, S.M., Divangahi, M., and Remold, H.G. (2010). Evasion of innate immunity by Mycobacterium tuberculosis: is death an exit strategy? Nat Rev Microbiol *8*, 668-674. 10.1038/nrmicro2387.

Behr, M.A., Edelstein, P.H., and Ramakrishnan, L. (2018). Revisiting the timetable of tuberculosis. BMJ *362*, k2738. 10.1136/bmj.k2738.

Behr, M.A., Edelstein, P.H., and Ramakrishnan, L. (2019). Is Mycobacterium tuberculosis infection life long? BMJ *367*, l5770. 10.1136/bmj.l5770.

Behr, M.A., Kaufmann, E., Duffin, J., Edelstein, P.H., and Ramakrishnan, L. (2021). Latent Tuberculosis: Two Centuries of Confusion. Am J Respir Crit Care Med *204*, 142-148. 10.1164/rccm.202011-4239PP.

Bendall, L.J., and Green, D.R. (2014). Autopsy of a cell. Leukemia *28*, 1341-1343. 10.1038/leu.2014.17.

Benjamin, D., Colombi, M., Moroni, C., and Hall, M.N. (2011). Rapamycin passes the torch: a new generation of mTOR inhibitors. Nat Rev Drug Discov *10*, 868-880. 10.1038/nrd3531.

Bento, C.F., Renna, M., Ghislat, G., Puri, C., Ashkenazi, A., Vicinanza, M., Menzies, F.M., and Rubinsztein, D.C. (2016). Mammalian Autophagy: How Does It Work? Annu Rev Biochem *85*, 685-713. 10.1146/annurev-biochem-060815-014556.

Berg, R.D., Levitte, S., O'Sullivan, M.P., O'Leary, S.M., Cambier, C.J., Cameron, J., Takaki, K.K., Moens, C.B., Tobin, D.M., Keane, J., and Ramakrishnan, L. (2016).

Lysosomal Disorders Drive Susceptibility to Tuberculosis by Compromising Macrophage Migration. Cell *165*, 139-152. 10.1016/j.cell.2016.02.034.

Berthet, F.X., Lagranderie, M., Gounon, P., Laurent-Winter, C., Ensergueix, D., Chavarot, P., Thouron, F., Maranghi, E., Pelicic, V., Portnoi, D., et al. (1998). Attenuation of virulence by disruption of the Mycobacterium tuberculosis erp gene. Science *282*, 759-762. 10.1126/science.282.5389.759.

Braverman, J., Sogi, K.M., Benjamin, D., Nomura, D.K., and Stanley, S.A. (2016). HIF-1alpha Is an Essential Mediator of IFN-gamma-Dependent Immunity to Mycobacterium tuberculosis. J Immunol *197*, 1287-1297. 10.4049/jimmunol.1600266.

Brodin, P., de Jonge, M.I., Majlessi, L., Leclerc, C., Nilges, M., Cole, S.T., and Brosch, R. (2005). Functional analysis of early secreted antigenic target-6, the dominant T-cell antigen of Mycobacterium tuberculosis, reveals key residues involved in secretion, complex formation, virulence, and immunogenicity. J Biol Chem *280*, 33953-33959. 10.1074/jbc.M503515200.

Cambier, C.J., Banik, S.M., Buonomo, J.A., and Bertozzi, C.R. (2020). Spreading of a mycobacterial cell-surface lipid into host epithelial membranes promotes infectivity. Elife *9*. 10.7554/eLife.60648.

Cambier, C.J., Falkow, S., and Ramakrishnan, L. (2014a). Host evasion and exploitation schemes of Mycobacterium tuberculosis. Cell *159*, 1497-1509. 10.1016/j.cell.2014.11.024.

Cambier, C.J., Takaki, K.K., Larson, R.P., Hernandez, R.E., Tobin, D.M., Urdahl, K.B., Cosma, C.L., and Ramakrishnan, L. (2014b). Mycobacteria manipulate macrophage

recruitment through coordinated use of membrane lipids. Nature *505*, 218-222. 10.1038/nature12799.

Canetti, G., Sutherland, I., and Svandova, E. (1972). Endogenous reactivation and exogenous reinfection: their relative importance with regard to the development of non-primary tuberculosis. Bull Int Union Tuberc *47*, 116-134.

Champion, M.M., Williams, E.A., Pinapati, R.S., and Champion, P.A. (2014). Correlation of phenotypic profiles using targeted proteomics identifies mycobacterial esx-1 substrates. J Proteome Res *13*, 5151-5164. 10.1021/pr500484w.

Chen, M., Divangahi, M., Gan, H., Shin, D.S., Hong, S., Lee, D.M., Serhan, C.N., Behar, S.M., and Remold, H.G. (2008). Lipid mediators in innate immunity against tuberculosis: opposing roles of PGE2 and LXA4 in the induction of macrophage death. J Exp Med *205*, 2791-2801. jem.20080767 [pii] 10.1084/jem.20080767.

Clay, H., Volkman, H.E., and Ramakrishnan, L. (2008). Tumor necrosis factor signaling mediates resistance to mycobacteria by inhibiting bacterial growth and macrophage death. Immunity *29*, 283-294.

Clemens, D.L., and Horwitz, M.A. (1995). Characterization of the Mycobacterium tuberculosis phagosome and evidence that phagosomal maturation is inhibited. J Exp Med *181*, 257-270. 10.1084/jem.181.1.257.

Conrad, W.H., Osman, M.M., Shanahan, J.K., Chu, F., Takaki, K.K., Cameron, J., Hopkinson-Woolley, D., Brosch, R., and Ramakrishnan, L. (2017). Mycobacterial ESX-1 secretion system mediates host cell lysis through bacterium contact-dependent gross

membrane disruptions. Proc Natl Acad Sci U S A *114*, 1371-1376. 10.1073/pnas.1620133114.

Cosma, C.L., Klein, K., Kim, R., Beery, D., and Ramakrishnan, L. (2006). Mycobacterium marinum Erp is a virulence determinant required for cell wall integrity and intracellular survival. Infect Immun *74*, 3125-3133. 74/6/3125 [pii] 10.1128/IAI.02061-05.

Cosma, C.L., Sherman, D.R., and Ramakrishnan, L. (2003). The secret lives of the pathogenic mycobacteria. Annu Rev Microbiol *57*, 641-676.

Cumming, B.M., Addicott, K.W., Adamson, J.H., and Steyn, A.J. (2018). Mycobacterium tuberculosis induces decelerated bioenergetic metabolism in human macrophages. Elife *7*. 10.7554/eLife.39169.

Cunningham, J.T., Rodgers, J.T., Arlow, D.H., Vazquez, F., Mootha, V.K., and Puigserver, P. (2007). mTOR controls mitochondrial oxidative function through a YY1-PGC-1alpha transcriptional complex. Nature *450*, 736-740. 10.1038/nature06322.

Davis, J.M., Clay, H., Lewis, J.L., Ghori, N., Herbomel, P., and Ramakrishnan, L. (2002). Real-time visualization of mycobacterium-macrophage interactions leading to initiation of granuloma formation in zebrafish embryos. Immunity *17*, 693-702.

Davis, J.M., and Ramakrishnan, L. (2009). The role of the granuloma in expansion and dissemination of early tuberculous infection. Cell *136*, 37-49.

Demy, D.L., Ranta, Z., Giorgi, J.M., Gonzalez, M., Herbomel, P., and Kissa, K. (2013). Generating parabiotic zebrafish embryos for cell migration and homing studies. Nature methods *10*, 256-258. 10.1038/nmeth.2362.

Deng, W., Yang, J., Lin, X., Shin, J., Gao, J., and Zhong, X.P. (2017). Essential Role of mTORC1 in Self-Renewal of Murine Alveolar Macrophages. J Immunol *198*, 492-504. 10.4049/jimmunol.1501845.

Divangahi, M., Chen, M., Gan, H., Desjardins, D., Hickman, T.T., Lee, D.M., Fortune, S., Behar, S.M., and Remold, H.G. (2009). Mycobacterium tuberculosis evades macrophage defenses by inhibiting plasma membrane repair. Nat Immunol *10*, 899-906. 10.1038/ni.1758.

Duvel, K., Yecies, J.L., Menon, S., Raman, P., Lipovsky, A.I., Souza, A.L., Triantafellow, E., Ma, Q., Gorski, R., Cleaver, S., et al. (2010). Activation of a metabolic gene regulatory network downstream of mTOR complex 1. Mol Cell *39*, 171-183. 10.1016/j.molcel.2010.06.022.

Edwards-Hicks, J., Mitterer, M., Pearce, E.L., and Buescher, J.M. (2020). Metabolic Dynamics of In Vitro CD8+ T Cell Activation. Metabolites *11*. 10.3390/metabo11010012.

Ehrt, S., Rhee, K., and Schnappinger, D. (2015). Mycobacterial genes essential for the pathogen's survival in the host. Immunol Rev *264*, 319-326. 10.1111/imr.12256.

Feldman, W.H., and Baggenstoss, A.H. (1938). The reisdual infectivity of the primary complex of tuberculosis. Am. J. Pathol. *14*, 473-490.

Fijalkowska-Morawska, J.B., Jagodzinska, M., and Nowicki, M. (2011). Pulmonary embolism and reactivation of tuberculosis during everolimus therapy in a kidney transplant recipient. Ann Transplant *16*, 107-110. 10.12659/aot.882226.

Fine-Coulson, K., Giguere, S., Quinn, F.D., and Reaves, B.J. (2015). Infection of A549 human type II epithelial cells with Mycobacterium tuberculosis induces changes in

mitochondrial morphology, distribution and mass that are dependent on the early secreted antigen, ESAT-6. Microbes Infect *17*, 689-697. 10.1016/j.micinf.2015.06.003.

Fortune, S.M., Jaeger, A., Sarracino, D.A., Chase, M.R., Sassetti, C.M., Sherman, D.R., Bloom, B.R., and Rubin, E.J. (2005). Mutually dependent secretion of proteins required for mycobacterial virulence. Proc Natl Acad Sci U S A *102*, 10676-10681. 10.1073/pnas.0504922102.

Galluzzi, L., Bravo-San Pedro, J.M., Kepp, O., and Kroemer, G. (2016). Regulated cell death and adaptive stress responses. Cell Mol Life Sci *73*, 2405-2410. 10.1007/s00018-016-2209-y.

Garcia, C.A., and Wu, S. (2016). Attributable Risk of Infection to mTOR Inhibitors Everolimus and Temsirolimus in the Treatment of Cancer. Cancer Invest *34*, 521-530. 10.1080/07357907.2016.1242009.

Garritano, S., Gemignani, F., Voegele, C., Nguyen-Dumont, T., Le Calvez-Kelm, F., De Silva, D., Lesueur, F., Landi, S., and Tavtigian, S.V. (2009). Determining the effectiveness of High Resolution Melting analysis for SNP genotyping and mutation scanning at the TP53 locus. BMC Genet *10*, 5. 10.1186/1471-2156-10-5.

Gleeson, L.E., Sheedy, F.J., Palsson-McDermott, E.M., Triglia, D., O'Leary, S.M., O'Sullivan, M.P., O'Neill, L.A., and Keane, J. (2016). Cutting Edge: Mycobacterium tuberculosis Induces Aerobic Glycolysis in Human Alveolar Macrophages That Is Required for Control of Intracellular Bacillary Replication. J Immunol *196*, 2444-2449. 10.4049/jimmunol.1501612.

Gonzalez, A., Hall, M.N., Lin, S.C., and Hardie, D.G. (2020). AMPK and TOR: The Yin and Yang of Cellular Nutrient Sensing and Growth Control. Cell Metab *31*, 472-492. 10.1016/j.cmet.2020.01.015.

Green, D.R., and Levine, B. (2014). To be or not to be? How selective autophagy and cell death govern cell fate. Cell *157*, 65-75. 10.1016/j.cell.2014.02.049.

Groschel, M.I., Sayes, F., Simeone, R., Majlessi, L., and Brosch, R. (2016). ESX secretion systems: mycobacterial evolution to counter host immunity. Nat Rev Microbiol *14*, 677-691. 10.1038/nrmicro.2016.131.

Guinn, K.M., Hickey, M.J., Mathur, S.K., Zakel, K.L., Grotzke, J.E., Lewinsohn, D.M., Smith, S., and Sherman, D.R. (2004). Individual RD1-region genes are required for export of ESAT-6/CFP-10 and for virulence of Mycobacterium tuberculosis. Mol Microbiol *51*, 359-370. 10.1046/j.1365-2958.2003.03844.x.

Halestrap, A.P. (1975). The mitochondrial pyruvate carrier. Kinetics and specificity for substrates and inhibitors. The Biochemical journal *148*, 85-96. 10.1042/bj1480085.

Harris, J., Hope, J.C., and Keane, J. (2008). Tumor necrosis factor blockers influence macrophage responses to Mycobacterium tuberculosis. J Infect Dis *198*, 1842-1850. 10.1086/593174.

He, C., Bartholomew, C.R., Zhou, W., and Klionsky, D.J. (2009). Assaying autophagic activity in transgenic GFP-Lc3 and GFP-Gabarap zebrafish embryos. Autophagy *5*, 520-526. 10.4161/auto.5.4.7768.

He, C., Holme, J., and Anthony, J. (2014). SNP genotyping: the KASP assay. Methods Mol Biol *1145*, 75-86. 10.1007/978-1-4939-0446-4_7.

Hinman, A.E., Jani, C., Pringle, S.C., Zhang, W.R., Jain, N., Martinot, A.J., and Barczak, A.K. (2021). Mycobacterium tuberculosis canonical virulence factors interfere with a late component of the TLR2 response. Elife *10*. 10.7554/eLife.73984.

Holscher, C., Reiling, N., Schaible, U.E., Holscher, A., Bathmann, C., Korbel, D., Lenz, I., Sonntag, T., Kroger, S., Akira, S., et al. (2008). Containment of aerogenic Mycobacterium tuberculosis infection in mice does not require MyD88 adaptor function for TLR2, -4 and -9. Eur J Immunol *38*, 680-694. 10.1002/eji.200736458.

Hopfner, K.P., and Hornung, V. (2020). Molecular mechanisms and cellular functions of cGAS-STING signalling. Nat Rev Mol Cell Biol *21*, 501-521. 10.1038/s41580-020-0244-x.

Hosoi, H., Dilling, M.B., Shikata, T., Liu, L.N., Shu, L., Ashmun, R.A., Germain, G.S., Abraham, R.T., and Houghton, P.J. (1999). Rapamycin causes poorly reversible inhibition of mTOR and induces p53-independent apoptosis in human rhabdomyosarcoma cells. Cancer Res *59*, 886-894.

Huang, L., Nazarova, E.V., Tan, S., Liu, Y., and Russell, D.G. (2018). Growth of Mycobacterium tuberculosis in vivo segregates with host macrophage metabolism and ontogeny. J Exp Med *215*, 1135-1152. 10.1084/jem.20172020.

Jamwal, S., Midha, M.K., Verma, H.N., Basu, A., Rao, K.V., and Manivel, V. (2013). Characterizing virulence-specific perturbations in the mitochondrial function of macrophages infected with Mycobacterium tuberculosis. Scientific reports *3*, 1328. 10.1038/srep01328.

Jeon, S.Y., Yhim, H.Y., Lee, N.R., Song, E.K., Kwak, J.Y., and Yim, C.Y. (2017). Everolimus-induced activation of latent Mycobacterium tuberculosis infection in a patient

with metastatic renal cell carcinoma. Korean J Intern Med *32*, 365-368. 10.3904/kjim.2015.121.

Karmaus, P.W.F., Herrada, A.A., Guy, C., Neale, G., Dhungana, Y., Long, L., Vogel, P., Avila, J., Clish, C.B., and Chi, H. (2017). Critical roles of mTORC1 signaling and metabolic reprogramming for M-CSF-mediated myelopoiesis. J Exp Med *214*, 2629-2647. 10.1084/jem.20161855.

Kettleborough, R.N., Busch-Nentwich, E.M., Harvey, S.A., Dooley, C.M., de Bruijn, E., van Eeden, F., Sealy, I., White, R.J., Herd, C., Nijman, I.J., et al. (2013). A systematic genome-wide analysis of zebrafish protein-coding gene function. Nature *496*, 494-497. 10.1038/nature11992.

Khattak, S., Murawala, P., Andreas, H., Kappert, V., Schuez, M., Sandoval-Guzman, T., Crawford, K., and Tanaka, E.M. (2014). Optimized axolotl (Ambystoma mexicanum) husbandry, breeding, metamorphosis, transgenesis and tamoxifen-mediated recombination. Nature protocols *9*, 529-540. 10.1038/nprot.2014.040.

Kiritsy, M.C., McCann, K., Mott, D., Holland, S.M., Behar, S.M., Sassetti, C.M., and Olive, A.J. (2021). Mitochondrial respiration contributes to the interferon gamma response in antigen-presenting cells. Elife *10*. 10.7554/eLife.65109.

Kozik, P., Gros, M., Itzhak, D.N., Joannas, L., Heurtebise-Chretien, S., Krawczyk, P.A., Rodriguez-Silvestre, P., Alloatti, A., Magalhaes, J.G., Del Nery, E., et al. (2020). Small Molecule Enhancers of Endosome-to-Cytosol Import Augment Anti-tumor Immunity. Cell reports *32*, 107905. 10.1016/j.celrep.2020.107905.

Lachmandas, E., Beigier-Bompadre, M., Cheng, S.C., Kumar, V., van Laarhoven, A., Wang, X., Ammerdorffer, A., Boutens, L., de Jong, D., Kanneganti, T.D., et al. (2016).

Rewiring cellular metabolism via the AKT/mTOR pathway contributes to host defence against Mycobacterium tuberculosis in human and murine cells. Eur J Immunol *46*, 2574-2586. 10.1002/eji.201546259.

Lee, J., Repasy, T., Papavinasasundaram, K., Sassetti, C., and Kornfeld, H. (2011). Mycobacterium tuberculosis induces an atypical cell death mode to escape from infected macrophages. PLoS One *6*, e18367. 10.1371/journal.pone.0018367.

Lee, P.Y., Sykes, D.B., Ameri, S., Kalaitzidis, D., Charles, J.F., Nelson-Maney, N., Wei, K., Cunin, P., Morris, A., Cardona, A.E., et al. (2017). The metabolic regulator mTORC1 controls terminal myeloid differentiation. Science immunology *2*. 10.1126/sciimmunol.aam6641.

Lerner, T.R., Queval, C.J., Fearns, A., Repnik, U., Griffiths, G., and Gutierrez, M.G. (2018). Phthiocerol dimycocerosates promote access to the cytosol and intracellular burden of Mycobacterium tuberculosis in lymphatic endothelial cells. BMC Biol *16*, 1. 10.1186/s12915-017-0471-6.

Levitte, S., Adams, K.N., Berg, R.D., Cosma, C.L., Urdahl, K.B., and Ramakrishnan, L. (2016). Mycobacterial Acid Tolerance Enables Phagolysosomal Survival and Establishment of Tuberculous Infection In Vivo. Cell Host Microbe *20*, 250-258. 10.1016/j.chom.2016.07.007.

Lienard, J., Nobs, E., Lovins, V., Movert, E., Valfridsson, C., and Carlsson, F. (2020). The Mycobacterium marinum ESX-1 system mediates phagosomal permeabilization and type I interferon production via separable mechanisms. Proc Natl Acad Sci U S A *117*, 1160-1166. 10.1073/pnas.1911646117.

Liu, G.Y., and Sabatini, D.M. (2020). mTOR at the nexus of nutrition, growth, ageing and disease. Nat Rev Mol Cell Biol *21*, 183-203. 10.1038/s41580-019-0199-y.

Manzanillo, P.S., Shiloh, M.U., Portnoy, D.A., and Cox, J.S. (2012). Mycobacterium tuberculosis activates the DNA-dependent cytosolic surveillance pathway within macrophages. Cell Host Microbe *11*, 469-480. 10.1016/j.chom.2012.03.007.

Mayer-Barber, K.D., Andrade, B.B., Oland, S.D., Amaral, E.P., Barber, D.L., Gonzales, J., Derrick, S.C., Shi, R., Kumar, N.P., Wei, W., et al. (2014). Host-directed therapy of tuberculosis based on interleukin-1 and type I interferon crosstalk. Nature *511*, 99-103. 10.1038/nature13489.

Mayer-Barber, K.D., Barber, D.L., Shenderov, K., White, S.D., Wilson, M.S., Cheever, A., Kugler, D., Hieny, S., Caspar, P., Nunez, G., et al. (2010). Caspase-1 independent IL-1beta production is critical for host resistance to mycobacterium tuberculosis and does not require TLR signaling in vivo. J Immunol *184*, 3326-3330. 10.4049/jimmunol.0904189.

Mercalli, A., Sordi, V., Ponzoni, M., Maffi, P., De Taddeo, F., Gatti, G., Servida, P., Bernardi, M., Bellio, L., Bertuzzi, F., et al. (2006). Rapamycin induces a caspase-independent cell death in human monocytes. Am J Transplant *6*, 1331-1341. 10.1111/j.1600-6143.2006.01332.x.

Mohareer, K., Medikonda, J., Vadankula, G.R., and Banerjee, S. (2020). Mycobacterial Control of Host Mitochondria: Bioenergetic and Metabolic Changes Shaping Cell Fate and Infection Outcome. Front Cell Infect Microbiol *10*, 457. 10.3389/fcimb.2020.00457.

Moreira-Teixeira, L., Mayer-Barber, K., Sher, A., and O'Garra, A. (2018). Type I interferons in tuberculosis: Foe and occasionally friend. J Exp Med *215*, 1273-1285. 10.1084/jem.20180325.

Morita, M., Gravel, S.P., Chenard, V., Sikstrom, K., Zheng, L., Alain, T., Gandin, V., Avizonis, D., Arguello, M., Zakaria, C., et al. (2013). mTORC1 controls mitochondrial activity and biogenesis through 4E-BP-dependent translational regulation. Cell Metab *18*, 698-711. 10.1016/j.cmet.2013.10.001.

Morita, M., Prudent, J., Basu, K., Goyon, V., Katsumura, S., Hulea, L., Pearl, D., Siddiqui, N., Strack, S., McGuirk, S., et al. (2017). mTOR Controls Mitochondrial Dynamics and Cell Survival via MTFP1. Mol Cell *67*, 922-935 e925. 10.1016/j.molcel.2017.08.013.

Mosimann, C., Kaufman, C.K., Li, P., Pugach, E.K., Tamplin, O.J., and Zon, L.I. (2011). Ubiquitous transgene expression and Cre-based recombination driven by the ubiquitin promoter in zebrafish. Development *138*, 169-177. 10.1242/dev.059345.

Mouton, J.M., Heunis, T., Dippenaar, A., Gallant, J.L., Kleynhans, L., and Sampson, S.L. (2019). Comprehensive Characterization of the Attenuated Double Auxotroph Mycobacterium tuberculosisDeltaleuDDeltapanCD as an Alternative to H37Rv. Front Microbiol *10*, 1922. 10.3389/fmicb.2019.01922.

Murphy, M.P. (2009). How mitochondria produce reactive oxygen species. The Biochemical journal *417*, 1-13. 10.1042/BJ20081386.

Muthukkumar, S., Ramesh, T.M., and Bondada, S. (1995). Rapamycin, a potent immunosuppressive drug, causes programmed cell death in B lymphoma cells. Transplantation *60*, 264-270. 10.1097/00007890-199508000-00010.

O'Neill, L.A., and Pearce, E.J. (2016). Immunometabolism governs dendritic cell and macrophage function. J Exp Med *213*, 15-23. 10.1084/jem.20151570.

Olson, G.S., Murray, T.A., Jahn, A.N., Mai, D., Diercks, A.H., Gold, E.S., and Aderem, A. (2021). Type I interferon decreases macrophage energy metabolism during mycobacterial infection. Cell reports *35*, 109195. 10.1016/j.celrep.2021.109195.

Ong, C.W., Elkington, P.T., and Friedland, J.S. (2014). Tuberculosis, pulmonary cavitation, and matrix metalloproteinases. Am J Respir Crit Care Med *190*, 9-18. 10.1164/rccm.201311-2106PP.

Opie, E.L., and Aronson, J.D. (1927). Tubercle bacilli in latent tuberculous lesions and in lung tissue without tuberculous lesions. Arch Pathol Lab Med *4*, 1-21.

Osman, M.M., Pagan, A.J., Shanahan, J.K., and Ramakrishnan, L. (2020). Mycobacterium marinum phthiocerol dimycocerosates enhance macrophage phagosomal permeabilization and membrane damage. PLoS One *15*, e0233252. 10.1371/journal.pone.0233252.

Osman, M.M., Shanahan, J.K., Chu, F., Takaki, K.K., Pinckert, M.L., Pagán, A.J., Brosch, R., Conrad, W.H., and Ramakrishnan, L. (2022). The C terminus of the mycobacterium ESX-1 secretion system substrate ESAT-6 is required for phagosomal membrane damage and virulence. Proc Natl Acad Sci U S A. (in press) *https://www.biorxiv.org/content/10.1101/2022.01.14.476355v1*.

Pagan, A.J., and Ramakrishnan, L. (2014). Immunity and Immunopathology in the Tuberculous Granuloma. Cold Spring Harbor perspectives in medicine *5*. 10.1101/cshperspect.a018499.

Pagan, A.J., and Ramakrishnan, L. (2018). The Formation and Function of Granulomas. Annu Rev Immunol *36*, 639-665. 10.1146/annurev-immunol-032712-100022.

Pagan, A.J., Yang, C.T., Cameron, J., Swaim, L.E., Ellett, F., Lieschke, G.J., and Ramakrishnan, L. (2015). Myeloid Growth Factors Promote Resistance to Mycobacterial Infection by Curtailing Granuloma Necrosis through Macrophage Replenishment. Cell Host Microbe *18*, 15-26. 10.1016/j.chom.2015.06.008.

Pajak, B., Siwiak, E., Soltyka, M., Priebe, A., Zielinski, R., Fokt, I., Ziemniak, M., Jaskiewicz, A., Borowski, R., Domoradzki, T., and Priebe, W. (2019). 2-Deoxy-d-Glucose and Its Analogs: From Diagnostic to Therapeutic Agents. Int J Mol Sci *21*. 10.3390/ijms21010234.

Pang, Z., Chong, J., Zhou, G., de Lima Morais, D.A., Chang, L., Barrette, M., Gauthier, C., Jacques, P.E., Li, S., and Xia, J. (2021). MetaboAnalyst 5.0: narrowing the gap between raw spectra and functional insights. Nucleic Acids Res *49*, W388-W396. 10.1093/nar/gkab382.

Patra, K.C., and Hay, N. (2014). The pentose phosphate pathway and cancer. Trends Biochem Sci *39*, 347-354. 10.1016/j.tibs.2014.06.005.

Paulson, T. (2013). Epidemiology: A mortal foe. Nature *502*, S2-3. 10.1038/502S2a.

Pernas, L. (2021). Cellular metabolism in the defense against microbes. J Cell Sci *134*. 10.1242/jcs.252023.

Powell, J.D., Pollizzi, K.N., Heikamp, E.B., and Horton, M.R. (2012). Regulation of immune responses by mTOR. Annu Rev Immunol *30*, 39-68. 10.1146/annurev-immunol-020711-075024.

Quigley, J., Hughitt, V.K., Velikovsky, C.A., Mariuzza, R.A., El-Sayed, N.M., and Briken, V. (2017). The Cell Wall Lipid PDIM Contributes to Phagosomal Escape and Host Cell Exit of Mycobacterium tuberculosis. mBio *8*. 10.1128/mBio.00148-17.

Ramakrishnan, L. (2012). Revisiting the role of the granuloma in tuberculosis. Nat Rev Immunol *12*, 352-366. 10.1038/nri3211.

Ramakrishnan, L. (2013). The zebrafish guide to tuberculosis immunity and treatment. Cold Spring Harb Symp Quant Biol *78*, 179-192. 10.1101/sqb.2013.78.023283.

Ramakrishnan, L. (2020). Mycobacterium tuberculosis pathogenicity viewed through the lens of molecular Koch's postulates. Curr Opin Microbiol *54*, 103-110. 10.1016/j.mib.2020.01.011.

Rambold, A.S., and Pearce, E.L. (2018). Mitochondrial Dynamics at the Interface of Immune Cell Metabolism and Function. Trends Immunol *39*, 6-18. 10.1016/j.it.2017.08.006.

Randow, F., and Youle, R.J. (2014). Self and nonself: how autophagy targets mitochondria and bacteria. Cell Host Microbe *15*, 403-411. 10.1016/j.chom.2014.03.012.

Roca, F.J., and Ramakrishnan, L. (2013). TNF dually mediates resistance and susceptibility to mycobacteria via mitochondrial reactive oxygen species. Cell *153*, 521-534. 10.1016/j.cell.2013.03.022.

Roca, F.J., Whitworth, L.J., Redmond, S., Jones, A.A., and Ramakrishnan, L. (2019). TNF Induces Pathogenic Programmed Macrophage Necrosis in Tuberculosis through a Mitochondrial-Lysosomal-Endoplasmic Reticulum Circuit. Cell *178*, 1344-1361 e1311. 10.1016/j.cell.2019.08.004.

Roca, F.J., Whitworth, L.J. , Prag, H.A., Murphy, M.P., and Ramakrishnan, L. (2022). TNF induces reverse electron transport through complex I to produce pathogenic mitochondrial reactive oxygen species and macrophage necrosis in tuberculosis. Submitted.

Ruiz-Camps, I., and Aguilar-Company, J. (2021). Risk of infection associated with targeted therapies for solid organ and hematological malignancies. Ther Adv Infect Dis *8*, 2049936121989548. 10.1177/2049936121989548.

Russell, D.G. (2007). Who puts the tubercle in tuberculosis? Nat Rev Microbiol *5*, 39-47.

Ryan, D.G., and O'Neill, L.A.J. (2020). Krebs Cycle Reborn in Macrophage Immunometabolism. Annu Rev Immunol *38*, 289-313. 10.1146/annurev-immunol-081619-104850.

Sampson, S.L., Dascher, C.C., Sambandamurthy, V.K., Russell, R.G., Jacobs, W.R., Jr., Bloom, B.R., and Hondalus, M.K. (2004). Protection elicited by a double leucine and pantothenate auxotroph of Mycobacterium tuberculosis in guinea pigs. Infect Immun *72*, 3031-3037. 10.1128/IAI.72.5.3031-3037.2004.

Sampson, S.L., Mansfield, K.G., Carville, A., Magee, D.M., Quitugua, T., Howerth, E.W., Bloom, B.R., and Hondalus, M.K. (2011). Extended safety and efficacy studies of a live attenuated double leucine and pantothenate auxotroph of Mycobacterium tuberculosis as a vaccine candidate. Vaccine *29*, 4839-4847. 10.1016/j.vaccine.2011.04.066.

Schieke, S.M., Phillips, D., McCoy, J.P., Jr., Aponte, A.M., Shen, R.F., Balaban, R.S., and Finkel, T. (2006). The mammalian target of rapamycin (mTOR) pathway regulates mitochondrial oxygen consumption and oxidative capacity. J Biol Chem *281*, 27643-27652. 10.1074/jbc.M603536200.

Shi, L., Salamon, H., Eugenin, E.A., Pine, R., Cooper, A., and Gennaro, M.L. (2015). Infection with Mycobacterium tuberculosis induces the Warburg effect in mouse lungs. Scientific reports *5*, 18176. 10.1038/srep18176.

Simeone, R., Bobard, A., Lippmann, J., Bitter, W., Majlessi, L., Brosch, R., and Enninga, J. (2012). Phagosomal rupture by Mycobacterium tuberculosis results in toxicity and host cell death. PLoS Pathog *8*, e1002507. 10.1371/journal.ppat.1002507.

Simeone, R., Sayes, F., Lawaree, E., and Brosch, R. (2021). Breaching the phagosome, the case of the tuberculosis agent. Cell Microbiol *23*, e13344. 10.1111/cmi.13344.

Sinclair, C., Bommakanti, G., Gardinassi, L., Loebbermann, J., Johnson, M.J., Hakimpour, P., Hagan, T., Benitez, L., Todor, A., Machiah, D., et al. (2017). mTOR regulates metabolic adaptation of APCs in the lung and controls the outcome of allergic inflammation. Science *357*, 1014-1021. 10.1126/science.aaj2155.

Small, J.L., O'Donoghue, A.J., Boritsch, E.C., Tsodikov, O.V., Knudsen, G.M., Vandal, O., Craik, C.S., and Ehrt, S. (2013). Substrate specificity of MarP, a periplasmic protease required for resistance to acid and oxidative stress in Mycobacterium tuberculosis. J Biol Chem *288*, 12489-12499. 10.1074/jbc.M113.456541.

Srinivasan, L., Ahlbrand, S., and Briken, V. (2014). Interaction of Mycobacterium tuberculosis with host cell death pathways. Cold Spring Harbor perspectives in medicine *4*. 10.1101/cshperspect.a022459.

Stanley, S.A., Johndrow, J.E., Manzanillo, P., and Cox, J.S. (2007). The Type I IFN response to infection with Mycobacterium tuberculosis requires ESX-1-mediated

secretion and contributes to pathogenesis. J Immunol *178*, 3143-3152. 10.4049/jimmunol.178.5.3143.

Sun, J., Siroy, A., Lokareddy, R.K., Speer, A., Doornbos, K.S., Cingolani, G., and Niederweis, M. (2015). The tuberculosis necrotizing toxin kills macrophages by hydrolyzing NAD. Nat Struct Mol Biol *22*, 672-678. 10.1038/nsmb.3064.

Suster, M.L., Abe, G., Schouw, A., and Kawakami, K. (2011). Transposon-mediated BAC transgenesis in zebrafish. Nature protocols *6*, 1998-2021. 10.1038/nprot.2011.416.

Swaim, L.E., Connolly, L.E., Volkman, H.E., Humbert, O., Born, D.E., and Ramakrishnan, L. (2006). Mycobacterium marinum infection of adult zebrafish causes caseating granulomatous tuberculosis and is moderated by adaptive immunity. Infect Immun *74*, 6108-6117.

Takaki, K., Davis, J.M., Winglee, K., and Ramakrishnan, L. (2013). Evaluation of the pathogenesis and treatment of Mycobacterium marinum infection in zebrafish. Nature protocols *8*, 1114-1124. 10.1038/nprot.2013.068.

Terplan, K. (1951). [Pathogenesis of postprimary tuberculosis, in relation to chronic pulmonary tuberculosis (phtisis)]. Bibl Tuberc *5*, 186-219.

Thomas, E.D., Cruz, I.A., Hailey, D.W., and Raible, D.W. (2015). There and back again: development and regeneration of the zebrafish lateral line system. Wiley Interdiscip Rev Dev Biol *4*, 1-16. 10.1002/wdev.160.

Tobin, D.M., Roca, F.J., Oh, S.F., McFarland, R., Vickery, T.W., Ray, J.P., Ko, D.C., Zou, Y., Bang, N.D., Chau, T.T., et al. (2012). Host genotype-specific therapies can optimize the inflammatory response to mycobacterial infections. Cell *148*, 434-446. 10.1016/j.cell.2011.12.023.

Tobin, D.M., Vary, J.C., Jr., Ray, J.P., Walsh, G.S., Dunstan, S.J., Bang, N.D., Hagge, D.A., Khadge, S., King, M.C., Hawn, T.R., et al. (2010). The lta4h locus modulates susceptibility to mycobacterial infection in zebrafish and humans. Cell *140*, 717-730. 10.1016/j.cell.2010.02.013.

Truett, G.E., Heeger, P., Mynatt, R.L., Truett, A.A., Walker, J.A., and Warman, M.L. (2000). Preparation of PCR-quality mouse genomic DNA with hot sodium hydroxide and tris (HotSHOT). BioTechniques *29*, 52, 54. 10.2144/00291bm09.

Tsai, M.K., Lee, C.Y., Hu, R.H., and Lee, P.H. (2007). Conversion to combined therapy with sirolimus and mycophenolate mofetil improved renal function in stable renal transplant recipients. J Formos Med Assoc *106*, 372-379. 10.1016/S0929-6646(09)60322-3.

van Ham, T.J., Mapes, J., Kokel, D., and Peterson, R.T. (2010). Live imaging of apoptotic cells in zebrafish. FASEB J *24*, 4336-4342. 10.1096/fj.10-161018.

Vandal, O.H., Pierini, L.M., Schnappinger, D., Nathan, C.F., and Ehrt, S. (2008). A membrane protein preserves intrabacterial pH in intraphagosomal Mycobacterium tuberculosis. Nat Med *14*, 849-854. 10.1038/nm.1795.

Volkman, H.E., Clay, H., Beery, D., Chang, J.C., Sherman, D.R., and Ramakrishnan, L. (2004). Tuberculous granuloma formation is enhanced by a mycobacterium virulence determinant. PLoS Biol *2*, e367.

Walton, E.M., Cronan, M.R., Beerman, R.W., and Tobin, D.M. (2015). The Macrophage-Specific Promoter mfap4 Allows Live, Long-Term Analysis of Macrophage Behavior during Mycobacterial Infection in Zebrafish. PLoS One *10*, e0138949. 10.1371/journal.pone.0138949.

Weichhart, T., Hengstschlager, M., and Linke, M. (2015). Regulation of innate immune cell function by mTOR. Nat Rev Immunol *15*, 599-614. 10.1038/nri3901.

Whitworth, L., Coxon, J., van Laarhoven, A., Thuong, N.T.T., Dian, S., Alisjahbana, B., Ganiem, A.R., van Crevel, R., Thwaites, G.E., Troll, M., et al. (2021a). A Bayesian analysis of the association between Leukotriene A4 Hydrolase genotype and survival in tuberculous meningitis. Elife *10*. 10.7554/eLife.61722.

Whitworth, L.J., Troll, R., Pagan, A.J., Roca, F.J., Edelstein, P.H., Troll, M., Tobin, D.M., Phu, N.H., Bang, N.D., Thwaites, G.E., et al. (2021b). Elevated cerebrospinal fluid cytokine levels in tuberculous meningitis predict survival in response to dexamethasone. Proc Natl Acad Sci U S A *118*. 10.1073/pnas.2024852118.

Wiens, K.E., and Ernst, J.D. (2016). The Mechanism for Type I Interferon Induction by Mycobacterium tuberculosis is Bacterial Strain-Dependent. PLoS Pathog *12*, e1005809. 10.1371/journal.ppat.1005809.

Wills, J., Edwards-Hicks, J., and Finch, A.J. (2017). AssayR: A Simple Mass Spectrometry Software Tool for Targeted Metabolic and Stable Isotope Tracer Analyses. Anal Chem *89*, 9616-9619. 10.1021/acs.analchem.7b02401.

Wong, Y.C., Ysselstein, D., and Krainc, D. (2018). Mitochondria-lysosome contacts regulate mitochondrial fission via RAB7 GTP hydrolysis. Nature *554*, 382-386. 10.1038/nature25486.

Zhang, L., Jiang, X., Pfau, D., Ling, Y., and Nathan, C.F. (2021). Type I interferon signaling mediates Mycobacterium tuberculosis-induced macrophage death. J Exp Med *218*. 10.1084/jem.20200887.

Zhang, Q., Wang, D., Jiang, G., Liu, W., Deng, Q., Li, X., Qian, W., Ouellet, H., and Sun, J. (2016). EsxA membrane-permeabilizing activity plays a key role in mycobacterial cytosolic translocation and virulence: effects of single-residue mutations at glutamine 5. Scientific reports *6*, 32618. 10.1038/srep32618.

Figure 1

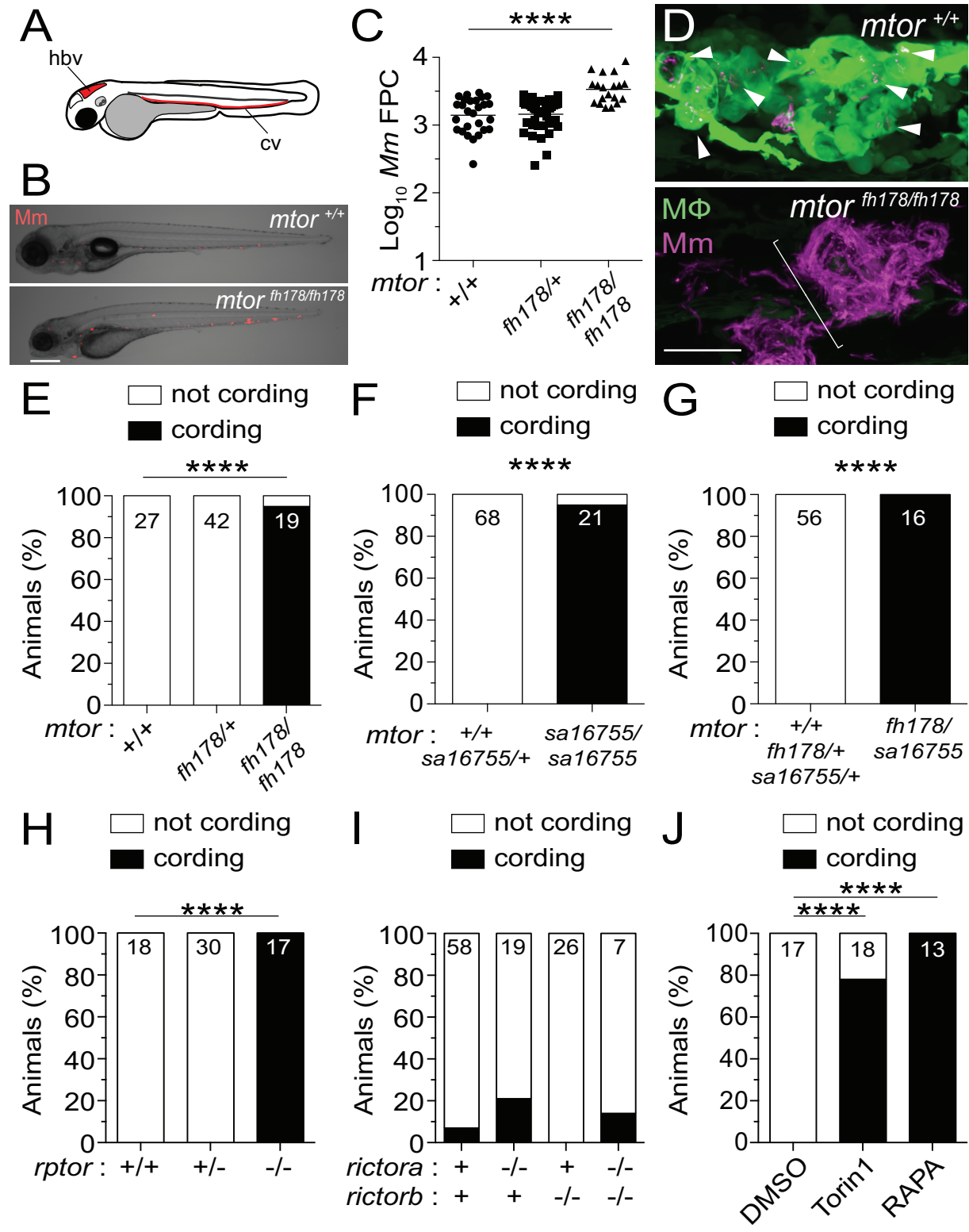
A
hbv
cv
B
Mm
mtor +/+
mtor fh178/fh178
C
****
Log10 Mm FPC
4
3
2
1
mtor :
+/+
fh178/+
fh178/ fh178
D
mtor +/+
MΦ
Mm
mtor fh178/fh178
E
not cording
cording
****
Animals (%)
100
80
60
40
20
0
27
42
19
mtor :
+/+
fh178/+
fh178/ fh178
F
not cording
cording
****
Animals (%)
68
21
mtor :
+/+ sa16755/+
sa16755/ sa16755
G
not cording
cording
****
Animals (%)
56
16
mtor :
+/+ fh178/+ sa16755/+
fh178/ sa16755
H
not cording
cording
****
Animals (%)
18
30
17
rptor :
+/+
+/-
-/-
I
not cording
cording
Animals (%)
58
19
26
7
rictora :
+
-/-
+
-/-
rictorb :
+
+
-/-
-/-
J
not cording
cording
****
****
Animals (%)
17
18
13
DMSO
Torin1
RAPA

Figure 2

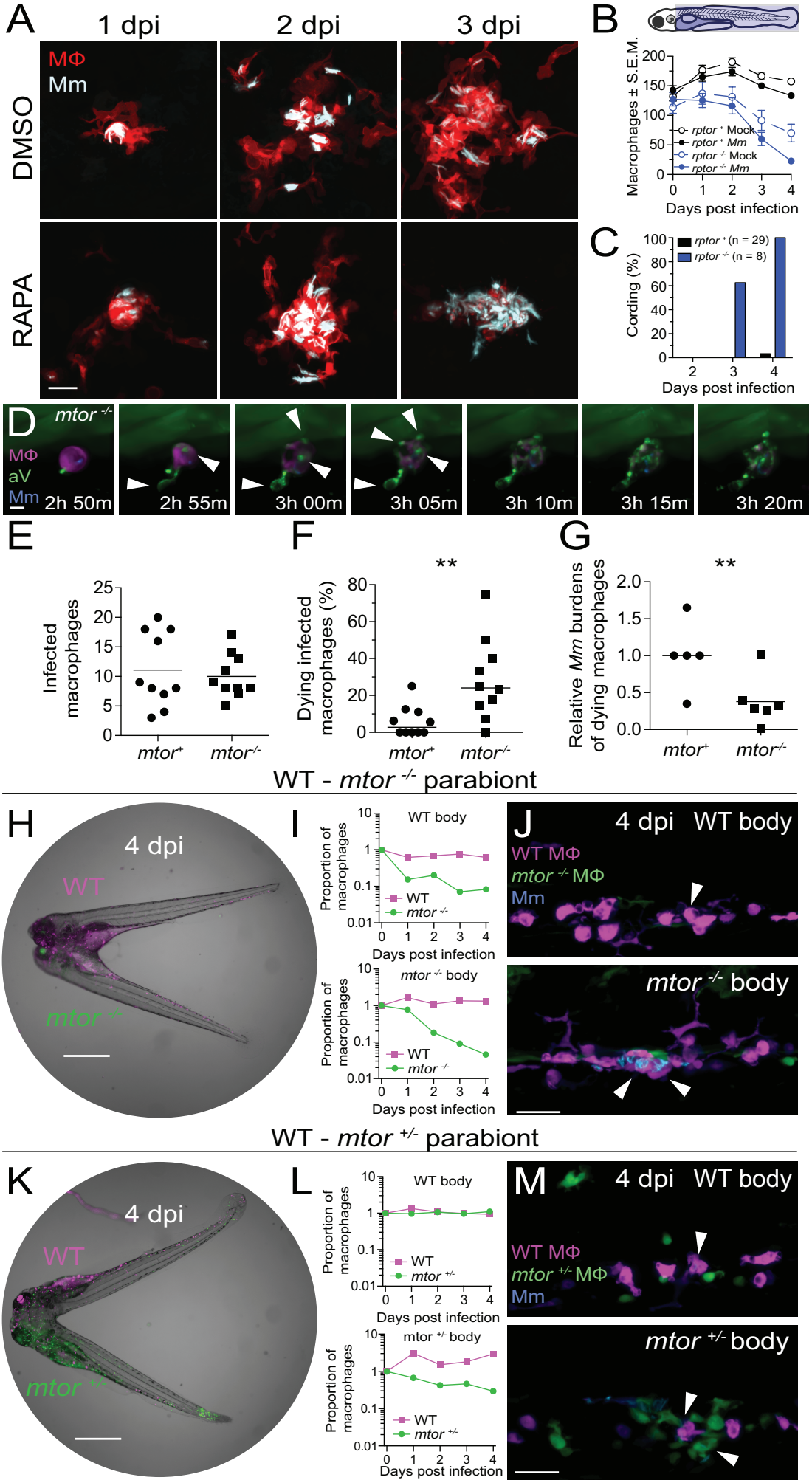
A
1 dpi
2 dpi
3 dpi
MΦ
Mm
DMSO
RAPA
B
Macrophages ± S.E.M.
rptor + Mock
rptor + Mm
rptor -/- Mock
rptor -/- Mm
Days post infection
C
Cording (%)
rptor + (n = 29)
rptor -/- (n = 8)
Days post infection
D
mtor -/-
MΦ
aV
Mm
2h 50m
2h 55m
3h 00m
3h 05m
3h 10m
3h 15m
3h 20m
E
Infected macrophages
mtor+
mtor-/-
F
Dying infected macrophages (%)
**
mtor+
mtor-/-
G
Relative Mm burdens of dying macrophages
**
mtor+
mtor-/-
WT - mtor -/- parabiont
H
4 dpi
WT
mtor -/-
I
WT body
Proportion of macrophages
WT
mtor -/-
Days post infection
mtor -/- body
Proportion of macrophages
WT
mtor -/-
Days post infection
J
4 dpi WT body
WT MΦ
mtor -/- MΦ
Mm
mtor -/- body
WT - mtor +/- parabiont
K
4 dpi
WT
mtor +/-
L
WT body
Proportion of macrophages
WT
mtor +/-
Days post infection
mtor +/- body
Proportion of macrophages
WT
mtor +/-
Days post infection
M
4 dpi WT body
WT MΦ
mtor +/- MΦ
Mm
mtor +/- body

Figure 3

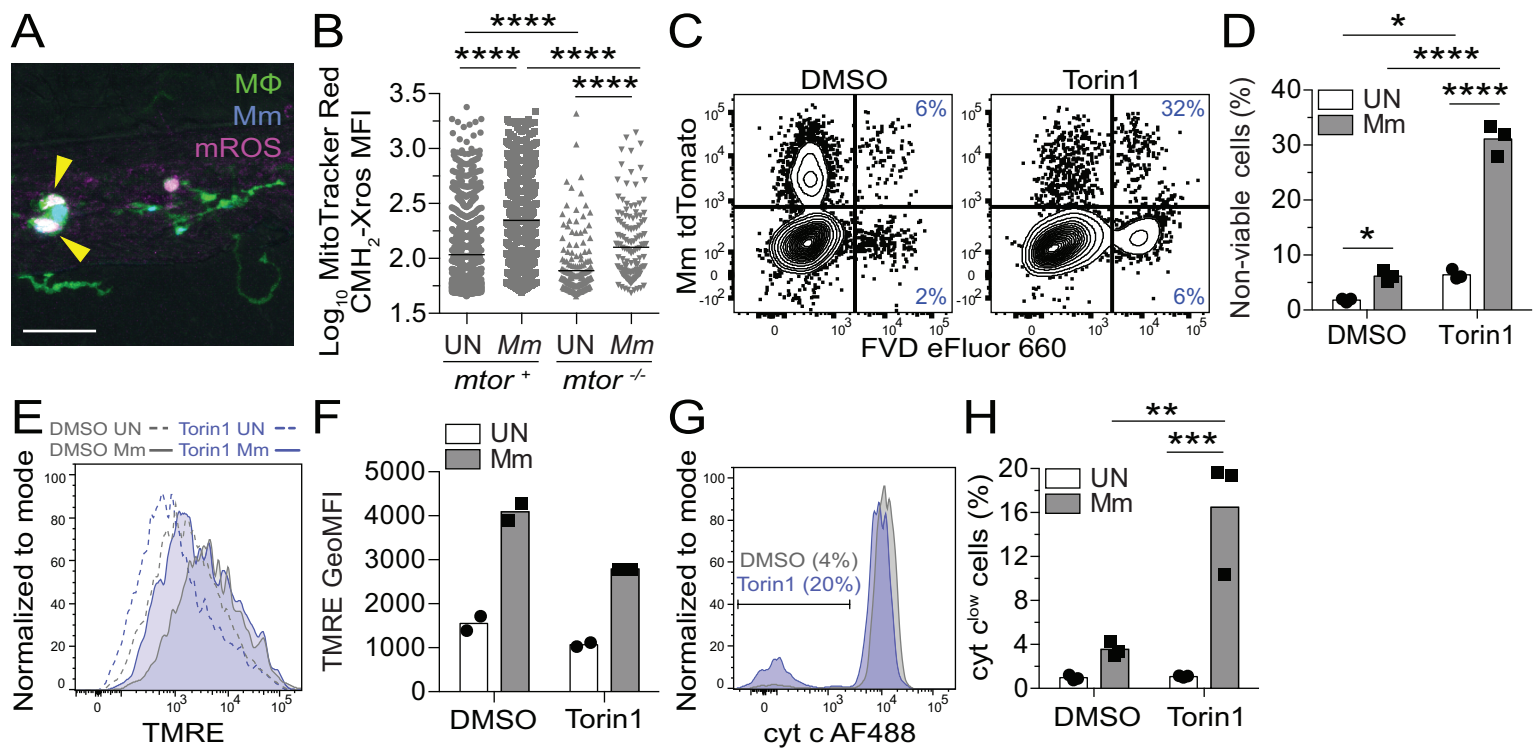
A
MΦ
Mm
mROS
B
Log10 MitoTracker Red CMH2-Xros MFI
UN
Mm
mtor +
mtor -/-
C
DMSO
Torin1
Mm tdTomato
FVD eFluor 660
6%
2%
32%
6%
D
Non-viable cells (%)
UN
Mm
DMSO
Torin1
E
DMSO UN
Torin1 UN
DMSO Mm
Torin1 Mm
Normalized to mode
TMRE
F
TMRE GeoMFI
UN
Mm
DMSO
Torin1
G
Normalized to mode
DMSO (4%)
Torin1 (20%)
cyt c AF488
H
cyt c low cells (%)
UN
Mm
DMSO
Torin1

Figure 4

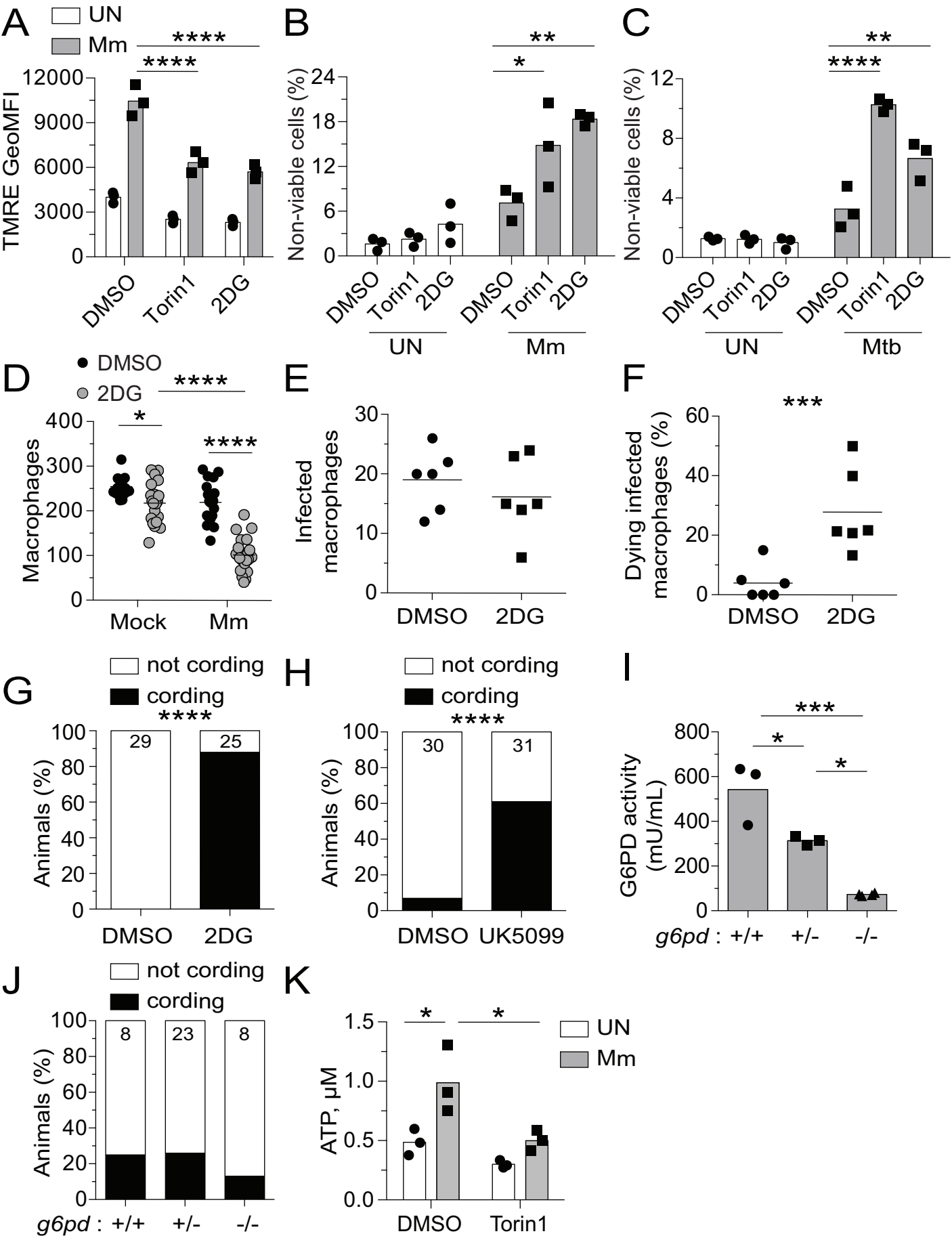
A
UN
Mm
****
****
TMRE GeoMFI
12000
9000
6000
3000
0
DMSO
Torin1
2DG
B
**
*
Non-viable cells (%)
24
18
12
6
0
DMSO
Torin1
2DG
DMSO
Torin1
2DG
UN
Mm
C
**
****
Non-viable cells (%)
12
8
4
0
DMSO
Torin1
2DG
DMSO
Torin1
2DG
UN
Mtb
D
DMSO
2DG
****
*
****
Macrophages
400
300
200
100
0
Mock
Mm
E
Infected macrophages
30
20
10
0
DMSO
2DG
F
***
Dying infected macrophages (%)
60
40
20
0
DMSO
2DG
G
not cording
cording
****
Animals (%)
100
80
60
40
20
0
29
25
DMSO
2DG
H
not cording
cording
****
Animals (%)
100
80
60
40
20
0
30
31
DMSO
UK5099
I
***
*
*
G6PD activity (mU/mL)
800
600
400
200
0
g6pd : +/+
+/-
-/-
J
not cording
cording
Animals (%)
100
80
60
40
20
0
8
23
8
g6pd : +/+
+/-
-/-
K
*
*
UN
Mm
ATP, µM
1.5
1.0
0.5
0.0
DMSO
Torin1

Figure 5

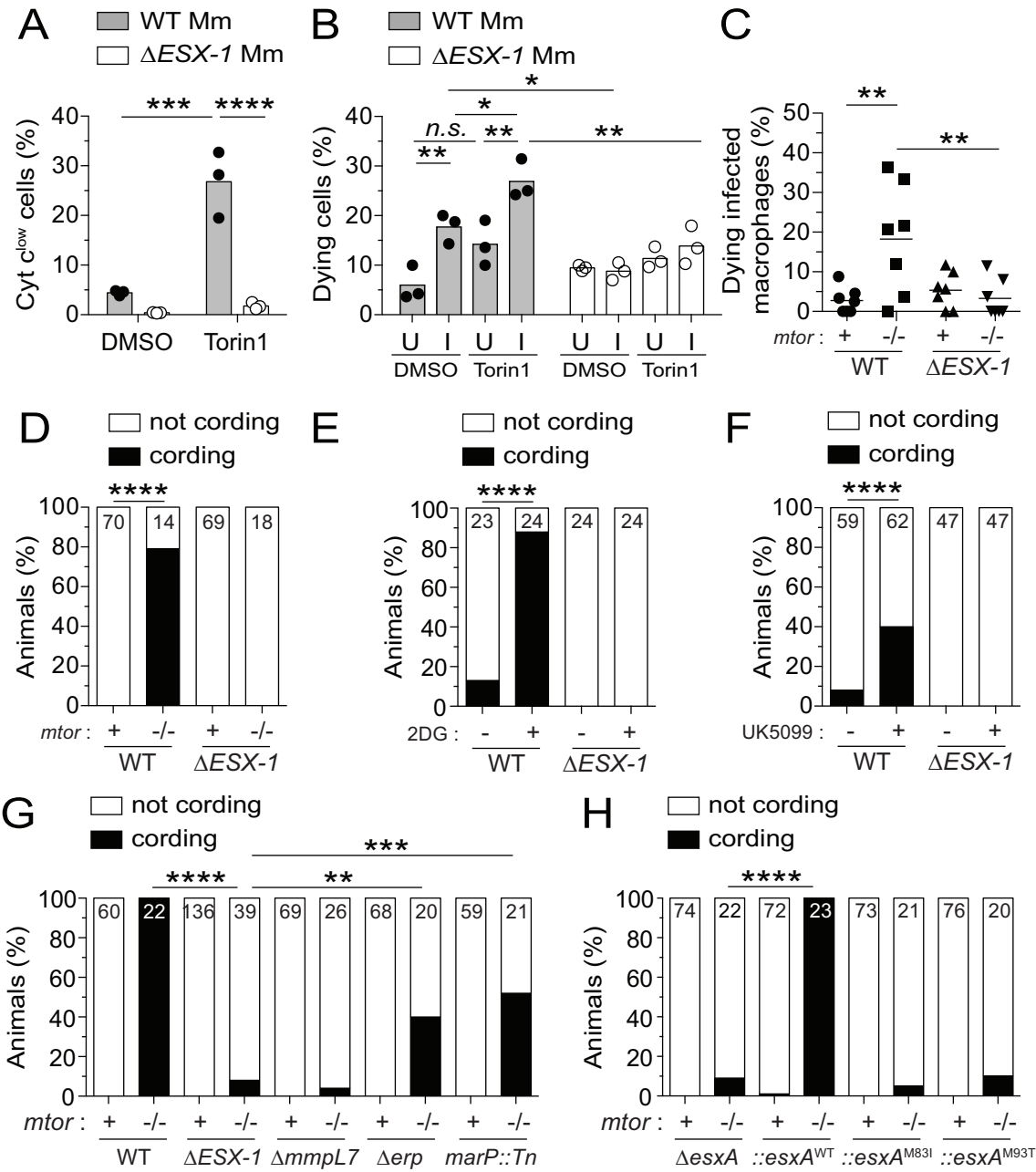
A
WT Mm
ΔESX-1 Mm
Cyt c^low cells (%)
***
****
DMSO
Torin1
B
WT Mm
ΔESX-1 Mm
Dying cells (%)
n.s.
**
*
U I U I U I U I
DMSO Torin1 DMSO Torin1
C
Dying infected macrophages (%)
mtor : + -/- + -/-
WT ΔESX-1
D
not cording
cording
Animals (%)
70 14 69 18
mtor : + -/- + -/-
WT ΔESX-1
E
23 24 24 24
2DG : - + - +
F
59 62 47 47
UK5099 : - + - +
G
60 22 136 39 69 26 68 20 59 21
ΔmmpL7 Δerp marP::Tn
H
74 22 72 23 73 21 76 20
ΔesxA ::esxA^WT ::esxA^M83I ::esxA^M93T

Figure 6

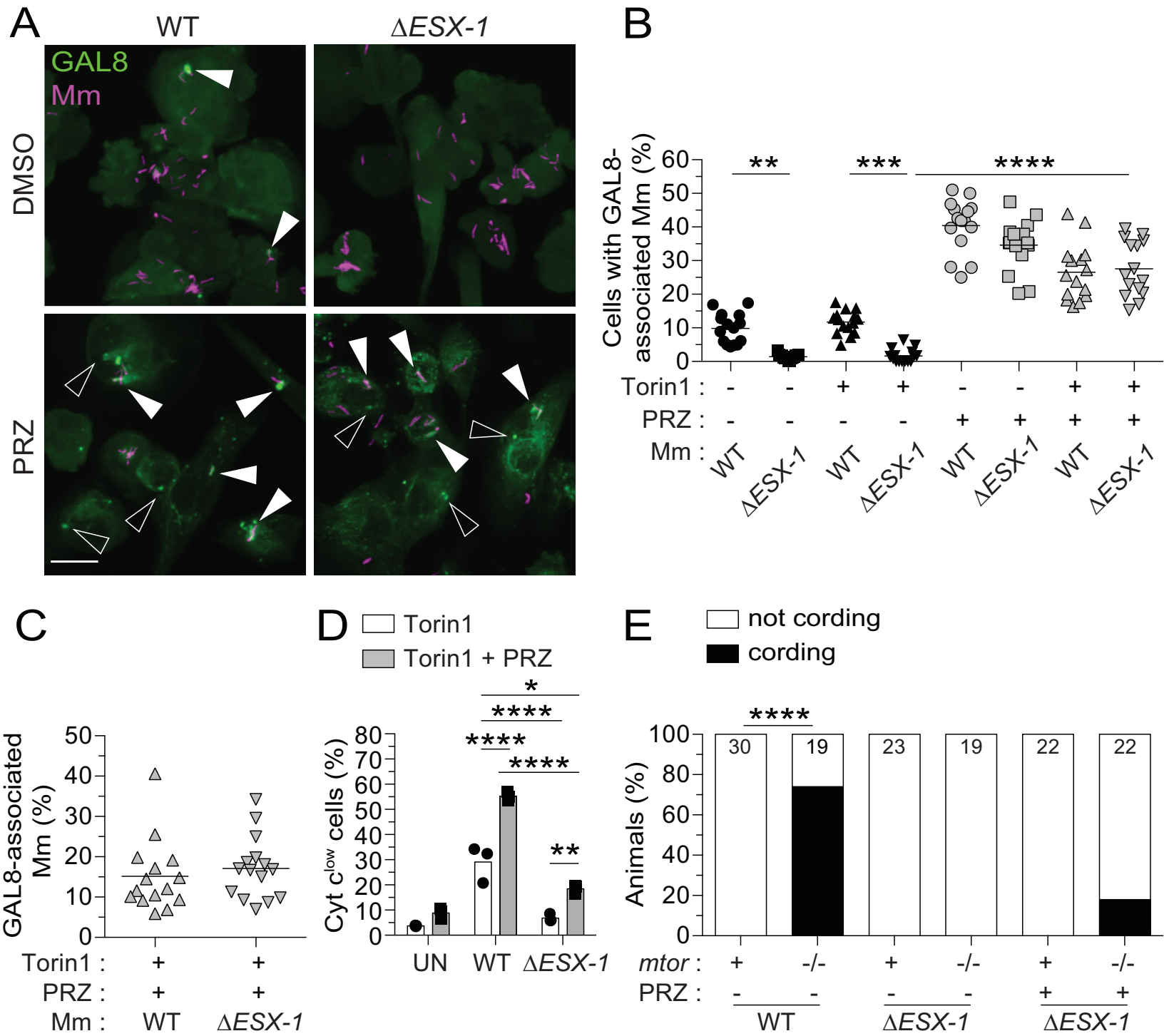
A
WT
ΔESX-1
GAL8
Mm
DMSO
PRZ
B
Cells with GAL8-associated Mm (%)
60
50
40
30
20
10
0
**
***
****
Torin1 : - - + + - - + +
PRZ : - - - - + + + +
Mm : WT ΔESX-1 WT ΔESX-1 WT ΔESX-1 WT ΔESX-1
C
GAL8-associated Mm (%)
50
40
30
20
10
0
Torin1 : + +
PRZ : + +
Mm : WT ΔESX-1
D
Torin1
Torin1 + PRZ
Cyt c^low cells (%)
80
70
60
50
40
30
20
10
0
*
****
****
****
**
UN WT ΔESX-1
E
not cording
cording
Animals (%)
100
80
60
40
20
0
****
30 19 23 19 22 22
mtor : + -/- + -/- + -/-
PRZ : - - - - + +
WT ΔESX-1 ΔESX-1

Figure 7

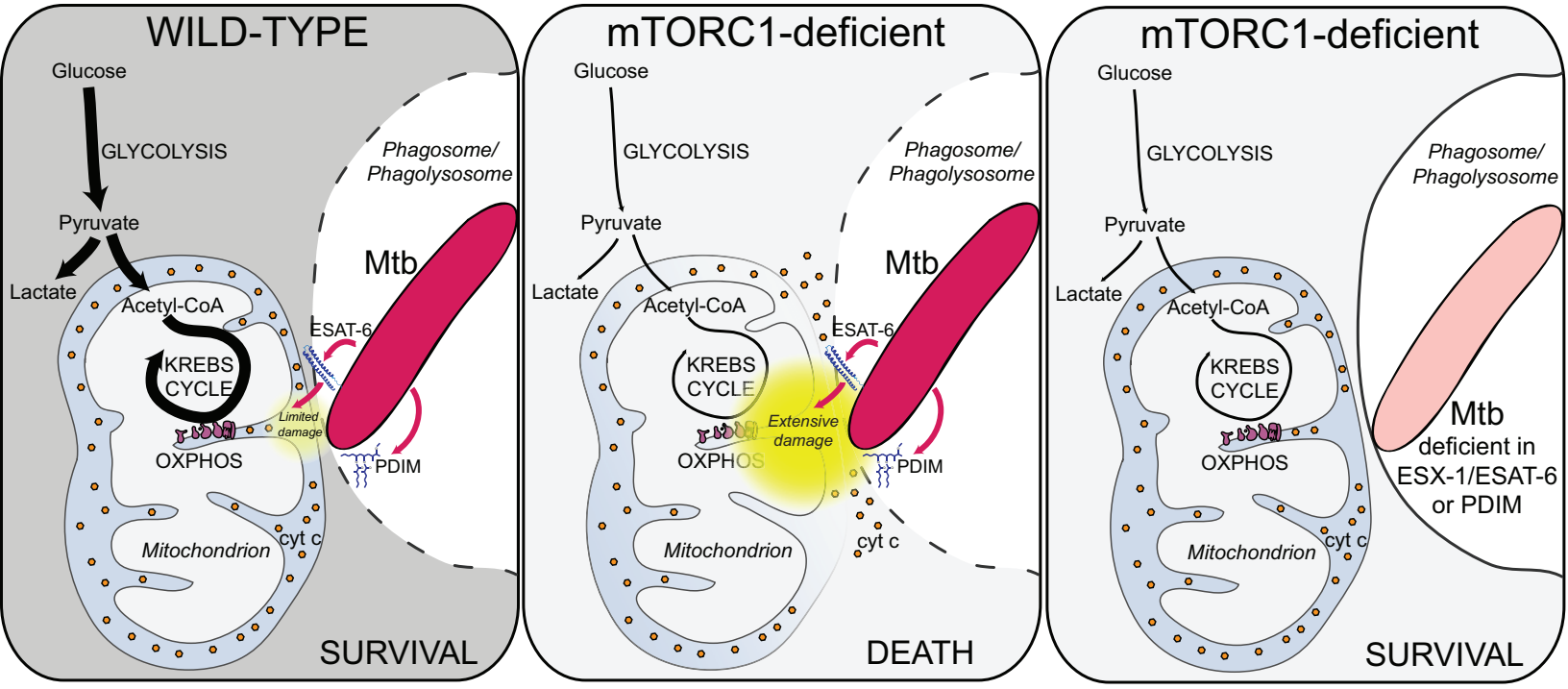
WILD-TYPE
Glucose
GLYCOLYSIS
Pyruvate
Lactate
Acetyl-CoA
KREBS CYCLE
OXPHOS
Mitochondrion
cyt c
Phagosome/ Phagolysosome
Mtb
ESAT-6
Limited damage
PDIM
SURVIVAL
mTORC1-deficient
Glucose
GLYCOLYSIS
Pyruvate
Lactate
Acetyl-CoA
KREBS CYCLE
OXPHOS
Mitochondrion
cyt c
Phagosome/ Phagolysosome
Mtb
ESAT-6
Extensive damage
PDIM
DEATH
mTORC1-deficient
Glucose
GLYCOLYSIS
Pyruvate
Lactate
Acetyl-CoA
KREBS CYCLE
OXPHOS
Mitochondrion
cyt c
Phagosome/ Phagolysosome
Mtb
deficient in ESX-1/ESAT-6 or PDIM
SURVIVAL